UNIVERSITA' DEGLI STUDI DI GENOVA

CEBR
CENTER OF EXCELLENCE FOR BIOMEDICAL RESEARCH

Dottorato di Ricerca in Immunologia Clinica e Sperimentale

(XXXII CICLO)

Biological and transcriptional regulation of the culprit in PDX lymphoma model

Coordinatore:
Prof.ssa Maria Cristina Mingari

Relatore:
Prof. Gilberto Filaci
Correlatore:
Prof. Giorgio Inghirami

Candidato:
Giuseppina Iliana Astone

ABSTRACT

The anaplastic large cell lymphoma (ALCL), a subtype of peripheral T-cell lymphoma (PTCL), is a lymphoid malignancy characterized by a "hallmark cells" and elevated expression of CD30. Anaplastic lymphoma kinase–positive (ALK+) carry ALK fusions, more often the NPM-*ALK* t(2;5) translocation, while about 40% of all ALCLs are negative (ALK-). ALK chimeras promote cell survival and tumorigenesis by constitutively activating multiple cell signaling pathways, including the STAT3 pathway. STAT3 is a member of family Signal Transducers and Activators of Transcription (STATs), and its chronic activation has been proven to play a role in the pathogenesis of several PTCL malignancies. Remarkably, approximately 50% of all ALK- ALCL have been proven to display the deregulated activation of the JAK-STAT3 pathway which is required for the maintenance of their neoplastic phenotype.

Here we described a series of pharmacological approaches designed to modulate the activity of STAT3 signaling. To achieve this objective, we have focused on ALK+ and ALK- ALCL cell lines and PDX models. We have taken advantage of two different but complementary molecules: a selective STAT3 binding compound named JPX-XX1, and two specific STAT3 degraders (A1 and N1). Both JPX-XX1 and A1 and N1 compounds were proven to reduce the cell growth and metabolic activity of ALK+ as well as selected ALK- ALCL cell lines, in a dose-dependent manner. As predicted both degraders were efficiently and selectively capable to degrade STAT3, a phenotype that was maintained over time (6 days of treatment) after a single dose exposure. Mechanistically, the loss of STAT3 was associated with a cell cycle arrest and increased apoptosis.

Collectively our data by confirming previous findings further demonstrate the pivotal role of STAT3 signaling in ALCL. More importantly, these compounds open new and feasible therapeutic avenues for the treatment of ALCL. A strategy that may be successfully applied to other JAK/STAT3 dependent lymphoproliferative disorders.

TABLE OF CONTENTS

ACRONYMS AND ABBREVIATIONS

7-AAD: 7-Amino-Actinomycin

Ab: Antibody

ALCL: Anaplastic Large Cell Lymphoma

ALK- ALK-negative

ALK: Anaplastic Lymphoma Kinase

ALK+: ALK-positive

ALO17: ALK Lymphoma Oligomerization Partner on Chromosome 17

AML: Acute Myeloid Leukemia

ATIC: 5-Aminoimidazole-4-Carboxamide Ribonucleotide Formyltransferase/IMP Cyclohydrolase

BIA-ALCL: Breast Implant Associated Lymphoma

CCD: Coiled-Coil Domain

CDX: Cancer-Derived Xenograft

CLTC-ALK: Clathrin Heavy Chain

CO2: Carbon dioxide

CRBN: Cereblon

DBD: DNA-Binding Domain

DMSO: Dimethyl Sulfoxide

E3: E3 ubiquitin ligase

EGFR: Epidermal Growth Factor Receptor

EML4: Echinoderm Microtubule-Associated Protein-Like 4

FBS: Fetal Bovine Serum

FFS: Failure Free Survival

HTS: High Throughput Sampler

HTS: High Throughput Sampler

IFN: Interferon

IGF-1RK: Insulin-Like Growth Factor Receptor

INSR: Insulin Receptor

IRK: Insulin Receptor Kinase

IRR: Insulin Receptor-Related Receptor

IRS1: Insulin Receptor Substrate-1

JAKs: Janus Kinases

JM: Juxtamembrane

KD: Kinase Domain

LTK: Leucocyte Tyrosine Kinase

MDK: Midkine

MetAp-2: Methionine Aminopeptidase-2

MOI: Multiplicity of Infection

MSN: Moesin

MYH9: Non-Muscle Myosin Heavy Chain

NHL: Non-Hodgkin Lymphoma

NMP: Nucleophosmin

NTD: Amino-Terminal Domain

OS: Overall Survival

PBS: Phosphate-Buffered Saline

PDGFR: Platelet-Derived Growth Factor Receptor

PDTX: Patient-Derived-Tumor-Xenograft

PI: Propidium Iodide

PI3K: Phosphatidylinositol 3 Kinase

PIAS: Protein Inhibitor of Activated STAT

POI: Protein of Interest

PROTACs: Proteolysis-Targeting Chimeras

PTCL: Peripheral T-Cell Lymphoma

PTN: Pleiotrophin

RTK: Receptor Tyrosine Kinase

S1PR: Sphingosine-1-Phosphate Receptor

SDS-PAGE: Sodium Dodecyl Sulphate-Polyacrylamide Gel Electrophoresis

SEM: Standard Error of the Mean

SH2: Src Homology-2

SHC: Src Homology 2 Domain Containing

SHC1: Shc Transforming Protein 1

SiRNA: small interfering Rna

SOCS: Suppressor of Cytokine Signaling

STATs: Family Signal Transducers and Activators of Transcription

TAD: Transactivation Domain

TFG: TRK-Fused Gene

TLRs: Toll Like Receptors

TPM3: Ttropomyosin 3

TPM4: Tropomyosin 4

UPS: Ubiquitin-Proteasome System

UT: untransduced

INTRODUCTION

Clinical and histological features of primary systemic ALCL.

Peripheral T-cell lymphoma (PTCL) is a lymphoma of post-thymic origin that represents approximately 12–15% of all non-Hodgkin lymphoma (NHL) in Western populations [1, 2]. In 1985 Stein and colleges first described anaplastic large cell lymphoma (ALCL), a subtype of PTCL, as a lymphoid malignancy characterized by marked cellular pleomorphism, propensity to grow cohesively, tendency to invade lymph node sinuses and diffuse expression of the Ki-1 antigen, later designated as CD30 [3]. In 1988, Fischer et al. first described chromosomal translocation affecting chromosomes 2 and 5 in a new Ki-1 positive lymphoma cell line called Karpas 299 [4]. In the next two years, several groups confirmed the association of this translocation to most of the Ki-1 positive lymphomas [5-7]. Just some years later, the product of t(2;5)(p23;q35) translocation was identified as the receptor tyrosine kinase (RTK) anaplastic lymphoma kinase (ALK) fused to nucleophosmin (NPM1, also known as NPM and B23) [8].

Nevertheless, ~40% of ALCL do not express ALK or other recurrent translocations. Although the current World Health Organization classification of lymphomas considers among the ALCL the following categories: ALK-positive (ALK+) and ALK-negative (ALK-) ALCL, meanwhile the breast associate ALCL remains a provisional entity. Cutaneous ALCL is included within the CD30 positive T-cell lymphoproliferative disorders [9]. The epidemiology of nodal ALCL is unique: ALK+ mostly occurs in pediatric patients, while ALK- occurs in older patients with a lower male predominance when compared to the previous one. Bone marrow, bone, subcutaneous tissue, and splenic involvement is seen at higher frequency in ALK+ patients, whereas skin, liver, and gastrointestinal involvement is more frequent in ALK- ALCL [10, 11].

Moreover, when treated with aggressive chemotherapy, patients affected by ALK+ ALCL have longer failure-free survival (FFS) and overall survival (OS) than ALK- ALCL patients (5-year OS: 70–80% vs. 33–49%) [10, 11].

ALCL typically shows a wide spectrum of morphologic features, ranging from small-cell neoplasms to cases where very large and anaplastic cells predominate. Almost all the cases, however, share a common feature, which is the presence of a variable number of so-called "hallmark cells" (Figure 1) [12, 13]. Specifically, these are large cells with abundant cytoplasm and "horseshoe" or "kidney-shaped" nuclei. Hallmark cells are usually large, but in the small-cell variants these elements are considerably smaller and more monotonous with pale cytoplasm, with a distinct cytoplasmic membrane and irregular nuclei mixed with some medium-size and large lymphoid cells.

Over with these highly characteristic and almost diagnostic hallmark cells, neoplastic elements with different morphology are usually seen. Common features of ALCL are an invasion of lymphatic sinuses and a perivascular pattern of neoplastic cell infiltration. An inflammatory background can be present, composed of abundant histiocytes with round–oval nuclei and eosinophilic cytoplasm, polymorphonuclear nuclear cells mixed with plasma cells, and rare leukocytes. In some cases (25%) significant fibrosis with collagenous bands suggestive of nodular sclerosis Hodgkin disease can be observed.
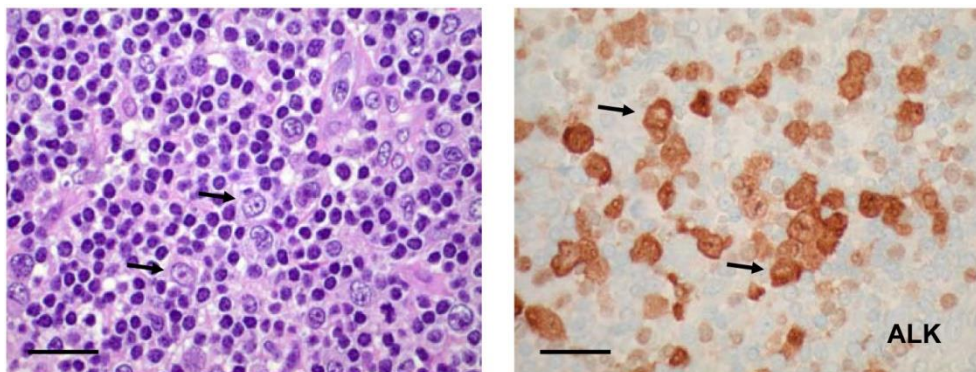

FIGURE 1- Typical hallmark cells of anaplastic large cell lymphoma [12]. *H&E staining on the left, ALK staining on the right.*

The CD30 antigen, a cytokine receptor of the tumor necrosis factor receptor superfamily, is strongly expressed by all. The staining pattern is typically membranous with strong reinforcement within the Golgi area. However, CD30 expression is not specific for ALCL and can be seen in activated non-neoplastic lymphoid cells, in a subset of B and T cell lymphoma, in Hodgkin's lymphoma and embryonal carcinoma.

ALCLs, present an abnormal phenotype with a variable positivity for several of T cell and non-T cell markers [14]. Despite the loss of the pan-T cell marker, all null ALCL by immunohistochemistry can usually be proven to be lymphoma of T-cell origin with clonal T-cell receptor-and -rearrangements. Among the pan-T-cell markers, only CD2 is most frequently positive, whereas CD3, CD5, CD7, andCD45RO are less detectable, with two or more of these negative or weakly positive. The CD4 and CD8 are variable and, in most cases, the tumor cells have a CD4+/CD8+pheno-type, but CD8+ cases have been described as well [10-12, 15]. Cytotoxic molecules such as granzyme B, perforin, and T-cell-restricted intracellular antigen-1 are almost always expressed.

The discovery of ALK translocations in ALCL has provided an objective tool for the recognition of some of these lymphomas. Because ALK expression, in the absence of translocations, has been documented in rare normal elements and some nonlymphoid neoplasms, positive ALK stains are highly informative. Indeed, the levels of expression of the ALK chimera in ALCL are quite high and fusion proteins can be easily detected using specific antibodies against ALK. ALK fusion protein expression is reproducibly demonstrated by immunohistochemistry in ~ 50% of systemic ALCL, whereas primary c-ALCL is always negative.

ALK, also known as CD246, belongs to the superfamily of insulin receptor kinase (IRK), which also includes the insulin-like growth factor receptor (IGF-1RK), the insulin receptor-related receptor (IRR), the insulin receptor (INSR), ROS and, at last, the leucocyte tyrosine kinase (LTK), which as a high structural homology with ALK, and constitutes a distinct subgroup within the IRKs [16, 17]. IRKs are an RTK with an extracellular ligand-binding domain, a transmembrane domain and a cytoplasmic kinase catalytic region. The extracellular region of ALK includes some motifs, including a 26-amino acid N-terminal signal peptide sequence, as well as the binding site (at residues 391-401) for the endogenous ligands pleiotrophin (PTN) and midkine (MDK) [18, 19]. The 28-amino acid transmembrane domain is followed by a 64-amino acid juxtamembrane (JM) domain, which contains a binding site of insulin receptor substrate-1 (IRS1), facilitating a tyrosine phosphorylation-dependent interaction. The Kinase Domain (KD) in the intracellular part includes a three-tyrosine-containing motif (Y1278, Y1282, Y1283) within its activation loop, representing the major self-phosphorylation site of the insulin receptor superfamily. The 244-amino acid

ALK C-terminus contains a phosphotyrosine-dependent binding site for the substrate protein SHC (Src homology 2 domain- containing) transforming protein 1 (SHC1), as well as an interaction site for phosphotyrosine-dependent binding of phospholipase C-c [20, 21].

ALK gene is composed of 26 exons; the 6226 bp cDNA encodes for a 177-kDa polypeptide that, after post-translational modifications, such as N-glycosylation, becomes a mature ALK RTK of approximately 200–220 kDa.

ALK receptor expression, originally documented in a variety of cancer lines, has been documented in many neuronal tumors [19, 22, 23], glioblastoma [24, 25] and mesenchymal neoplasms including melanoma [26] and rhabdomyosarcoma [8, 27, 28].

In this context, ALK overexpression or gain of function mutations have been demonstrated to be tumorigenic. ALK expression in hematological disorders ALCL, first described in 1985 [3].

NPM-ALK in ALCL

Many ALK-positive (ALK+) ALCL, around the 90%, express the NPM–ALK fusion protein, derived from the t(2;5)(p23;q25) translocation [13]. NPM is a multifunctional protein: acts as a molecular chaperone in the transport of pre-ribosomal particles from the nucleus to the cytoplasm. Moreover, it plays a critical role in DNA repair, transcription, and genomic stability as well [29]. The N-terminus domain of NPM, within the ALK chimera, provides a dimerization domain, essential for chimera autophosphorylation, allowing the constitutive activation of the kinase and the firing of downstream signaling [9, 30, 31].

The oncogenic potential role of ALK chimeras was first demonstrated in vivo by Kuefer and colleagues, subjecting mice to bone marrow transplantation with cells transduced with NPM–ALK constructs [32]. One year later, similar results were obtained in vitro testing the transforming potential of fibroblasts containing NPM–ALK [33]. However, it was in 2003 that the lymphomagenic role of NPM–ALK was confirmed by generation of a mouse model in which the expression of NPM-ALK showed the spontaneous development of T-cell lymphomas and/or plasmacytoma [34]; confirmed than by Turner and Alexander by using additional mouse models [35]. Several studies have identified that NPM–ALK

promotes cell survival and tumorigenesis by constitutively activating many cell signaling pathways (Figure 2), including the STAT pathway [9].

ALK-dependent mitogenic signaling is largely mediated via Ras/MAP kinase pathway through the direct binding of IRS1, SHC, and SRC on specific tyrosine residues within the intracytoplasmic segment of ALK. The SHP2/GRB2 complex interacts with p130Cas, modifying the cytoskeleton organization as well. In the case of ALK-driven phosphatidylinositol 3 kinase (PI3K) activation, a relevant anti-apoptotic signal is generated mainly through pAKT1/2, and its downstream molecules (inhibition of BAD and FOXO3a-mediated transcription). At the same time, the PI3K pathway controls cell cycle progression. An additional oncogenic signal may be provided by PLC-g, which binds directly to activated ALK, and generating diacylglycerol and IP3 activates PKC and mobilizes calcium stores from the endoplasmic reticulum [9].

A critical oncogenic player is represented by the JAK/STAT3 pathway, which provides essential survival signals and modulates the cellular metabolism regulating the mitochondrial oxidation chain. The downstream effectors of STAT3 include several members of the BCL2 family (BCL2, BCL-XL, and MCL-1) and anti-apoptotic proteins, as survivin and multiple transcription factors (as C/EBPb).
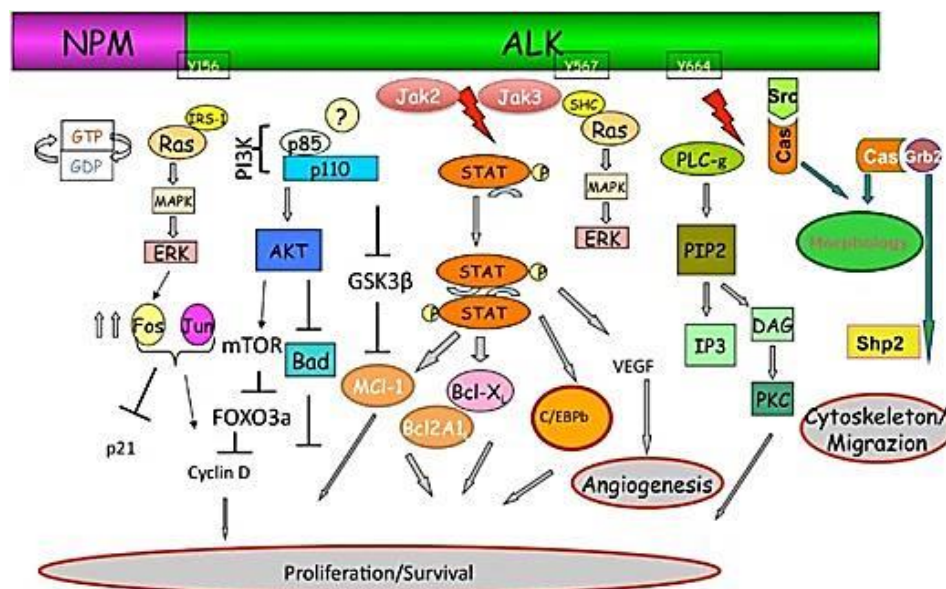

FIGURE 2 – NMP-ALK and its signaling transduction pathways [36].

Once STATs are phosphorylated, they dimerize and accumulate in the cell nucleus and bind to enhancer elements of target genes. Zamo and colleagues [37] have first shown that STAT3 is the key effector molecule of the ALK-mediated signaling in ALCL and its activation is required for the maintenance of the neoplastic phenotype [38]. NPM–ALK can directly phosphorylate STAT3 or can activate JAK3, which in turn can contribute to STAT3 activation [9]. STAT3 phosphorylation in tyr705 results in an increased expression of BCL2, BCL-XL, survivin, and MCL-1 proteins, involved in anti-apoptotic processes. STAT3-mediated signal also leads to uncontrolled proliferation, acting on cell cycle regulators such as cyclin D3 and c-myc, often overexpressed in ALK+ lymphoma [34, 39].

Cooperation between NPM–ALK and JAK/STAT pathway might also lead in a certain context to the STAT5 activation, although in T-cell, STAT3 acts as a STAT5 repressor [40, 41].

ALK fusion proteins

In addition to NPM–ALK, many other fusion proteins can be expressed in ALCL, namely ALK lymphoma oligomerization partner on chromosome 17 (ALO17), TRK-fused gene (TFG), moesin (MSN), tropomyosin 3 and 4 (TPM3 and TPM4), 5-aminoimidazole-4-carboxamide ribonucleotide formyltransferase/IMP cyclohydrolase (ATIC), non-muscle myosin heavy chain (MYH9), and clathrin heavy chain (CLTC–ALK) [36]. Moreover, ALK rearrangements have also been detected in large B-cell lymphoma and various tumors of mesenchymal and epithelial origin, including inflammatory myofibroblastic tumors, lung cancer, esophageal squamous cell carcinoma and others [42]. Notably, the same ALK fusions, such as TPM3-ALK, TPM4-ALK, TFG-ALK, SEC31A-ALK, ATIC-ALK, CLTC-ALK and EML4 (echinoderm microtubule-associated protein-like 4) -ALK occur in ALK+ malignancies of different cells of origin, highlighting the crucial role of ALK in tumorigenesis [42, 43]. Collectively, these discoveries have encouraged the development of therapeutic strategies regarding ALK+ tumors.

In 2003, Hubinger and colleagues performed the ablation of ALK protein expression, obtained by ALK-specific small interfering RNA (siRNA) duplexes or selective ribozyme [44]. This study showed that the ALK knockdown leads first to a cell cycle arrest, followed by massive apoptosis in vitro and in vivo some

years later [45]. Results that were confirmed applying ALK-specific small molecules [46, 47] and subsequently were supported by other novel ATP-competitive inhibitors [48, 49]. Really important was the discovery of specific ALK tyrosine inhibitors, one of which, crizotinib, has proven to have clinical efficacy in the treatment of ALK+ non-small cell lung cancer and ALCL [50, 51]. Crizotinib (PF-02341066) is a dual MET/ALK inhibitor, that binds into the nucleotide pocket of the target kinase and prevents ATP from binding to the enzyme [52]. Originally, crizotinib was developed as a selective c-MET inhibitor and indeed it showed excellent anti-tumor activity in MET-dependent cancer models [52, 53]. While selectivity profiling of the compound was performed, ALK resulted as another substrate sensible to the drug. Hence, the drug was then studied as an ALK inhibitor [54].

Afterward, other small molecules have reached the clinics, as LDK378, or the pre-clinical stages as CEP28122, CEP37440, AP-26113, and more [55].

Since ALK signaling activates multiple downstream molecules, it could be also useful to use molecules that can target effectors involved in this pathway to treat ALK+ cancer patients. Considering the oncogenetic addition of ALK+ ALCL to STAT3, inhibition of this transcription factor could provide a therapeutic target [45].

Signal Transducers and Activators of Transcription 3 (STAT3)

STAT3 is an important member of family Signal Transducers and Activators of Transcription (STATs), that regulates gene transcription that transmits signals from activated plasma membrane receptors to the nucleus in response to various stimuli [56, 57].

STATs were first discovered in 1994 and found to be involved in interferon (IFN)-triggered transcription regulation [58]. Seven different STAT proteins, namely STAT1, -2, -3, -4, -5a, -5b, and -6, have been discovered in mammalian cells [59]. These proteins can transduce intracellular and extracellular signals that mediate multiple cellular functions related to survival, growth, proliferation, and angiogenesis [60, 61]. Commonly localized in the cytoplasmic compartment of the cell, STATs are present in an inactive state, either as monomers or as

unphosphorylated dimers that can be activated by various stimuli such as cytokines and growth factors [62, 63].

Upstreaming STATs are activated by phosphorylation on tyrosine by Janus kinases (JAKs), Src family members, as well as growth factor receptors such as epidermal growth factor receptor (EGFR) and platelet-derived growth factor receptor (PDGFR) [59, 64]. The crystal structure of STAT3-ß bound to a DNA molecule (Figure 3) was determined in 1998, offering insight into STAT3 function and steps necessary to transduce the signal into transcriptional activation [65].
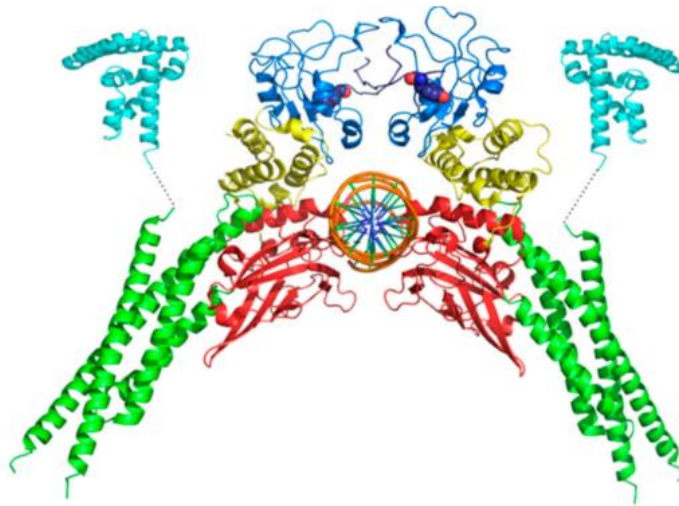

FIGURE 3 – Crystal structure of STAT3β [66]. *Color keys: cyan = amino-terminal domain; green = coiled-coil domain; red = DNA-binding domain; yellow = linker domain; blue = SH2 domain; violet = transactivation domain; orange = DNA. Tyrosine 705 residues are shown as spheres.*

STAT3 consists of 770 amino acids that constitute six different functional domains, including amino-terminal domain (NTD), coiled-coil domain (CCD), DNA-binding domain (DBD), linker domain, SH2 domain, and the carboxyl-terminal transactivation domain (TAD) (Figure 4).
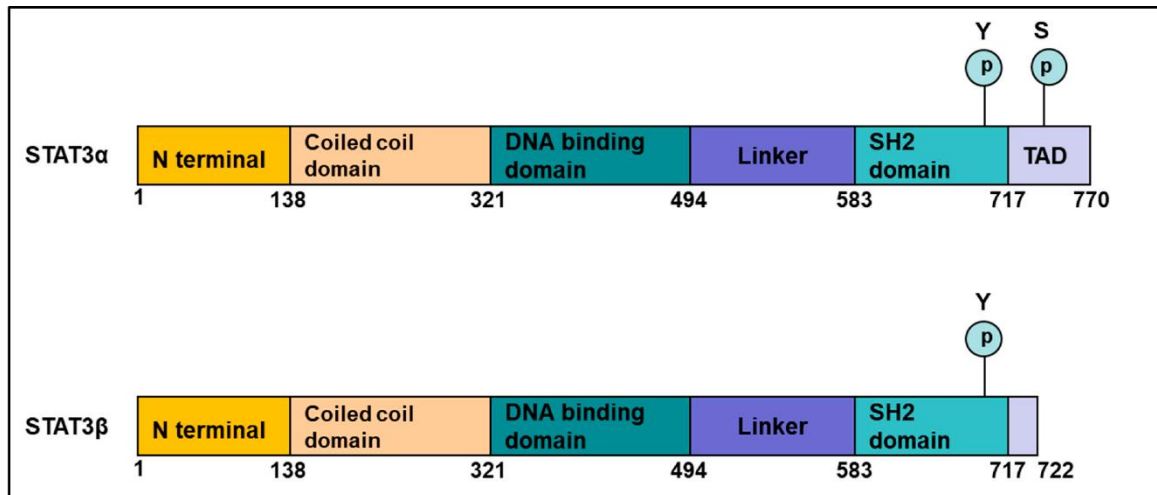
FIGURE 4 –The molecular structure of the two STAT3 isoforms [67].

The NTD is essential for the cooperative binding of STATs to multiple consensus DNA sites. The CCD is critical for the recruitment of STAT3 to the receptor and subsequent phosphorylation, dimerization; also, residues essential for nuclear translocation are contained. The DBD can recognize a specific molecular motif in the DNA. The SH2 domain is important for recruitment and activation and dimerization of the STAT3 molecule by interacting with phosphorylated tyrosine residues (Tyr705). The TAD differs between α and β isoforms (Figure 4), with the β form having a unique truncated C-terminal sequence. In this domain is locate Tyr705 becomes phosphorylated upon activation of STAT3. An additional phosphorylation site within the TAD, Serine 727 (Ser727) is important for regulating STAT3 activation by serine/threonine kinases such as the MAPKs (mitogen-activated protein kinases) [67, 68].

STAT3 is activated by binding of a ligand to its receptor on the cell surface. Ligand binding leads to activation of JAK, which recruits and phosphorylates STAT3. STAT3 then forms a dimer, moves into the nucleus and controls transcription. Upstream signals that can trigger JAK kinase-mediated phosphorylation on Y705 (YP) range from cytokines of the IL-6 family, leptin, IL-12, IL-17, IL-10, interferons, growth factors such as G-CSF, EGF, PDGF, and some oncogenes, the prototype of which is Src family kinases but also including Abl, Sis, Fps, Ros, Met and ErbB2 [69-71]. Moreover, G protein-coupled

receptors, like the sphingosine-1-phosphate receptor (S1PR) 1, and several toll-like receptors (TLRs) have been shown to activate STAT3[69, 72].
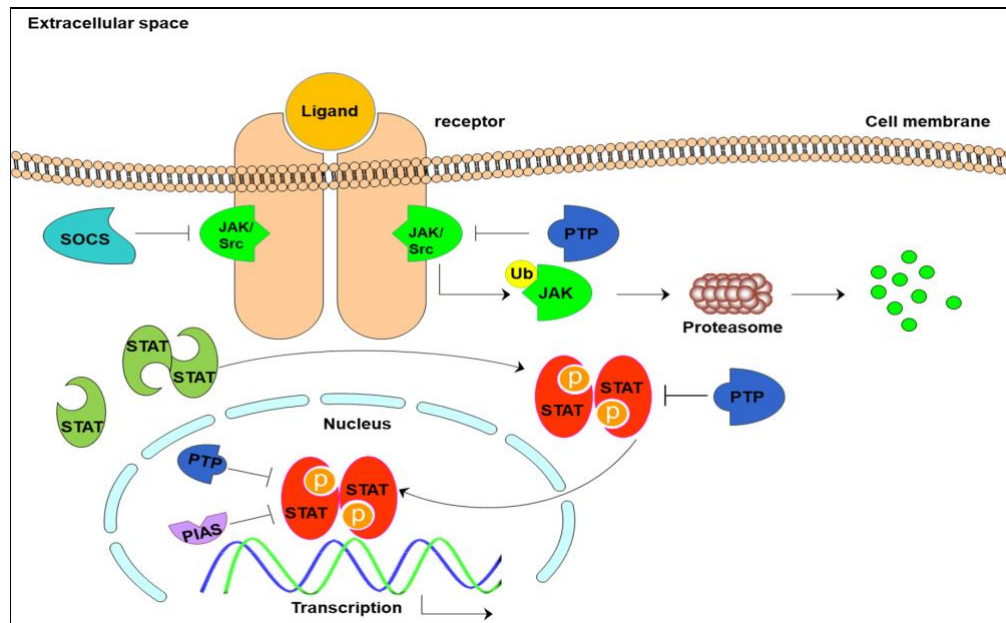

FIGURE 5 – Schematic representation of STAT3 signaling cascade [67].

In physiological conditions, STAT3 activation is controlled by three groups of negative regulators: phosphatases, suppressor of cytokine signaling (SOCS) proteins, and protein inhibitor of activated STAT (PIAS) proteins [73, 74]. Phosphatases like SHP-1, SHP-2, PTP1B or T cell PTP terminate STAT3 activation, acting either at the level of JAK kinases or directly in the nucleus [73]. SOCS3, of SOCS family, is a primary transcriptional target of STAT3 and acts as a negative feedback regulator to inhibit JAK activity, while PIAS3 prevents the binding of STAT3 to its target DNA sequence [75, 76]. Chronic STAT3 activation in tumors is known to occur downstream of aberrant upstream stimulation [77]. Furthermore, STAT3 somatic mutations have been shown to play a role in the pathogenesis of hematopoietic malignancies [78, 79]. Recently, recurrent mutation is discovered in ALK- ALCL panel, suggesting that a STAT3-mediated oncogenic mechanism may be shared by all ALCLs, independent of ALK status. Mutation recurrence of JAK/STAT3 genes in ALK-ALCL was largely studied by Inghirami's team that sequenced 155 primary ALCL samples (between ALK- and ALK+) and 74 PTCLs (included angioimmunoblastic

17

T cell lymphomas, PTCLs not otherwise specified [PTCL-NOS], and NK-T cell lymphomas) [80].

Innovative therapeutic approaches for STAT3 target

Despite the role of STAT3 as a potential therapeutic target, the development of STAT3 inhibitors for clinical use has been slow.

Inhibition of the up-stream pathway as JAK kinase can decrease the phosphorylation and activity of STAT3. However, the use of this kind of inhibitors, such as ruxolitinib, has a relatively weak effect on STAT3 and demonstrates only a modest clinical benefit in patients with STAT3-driven malignancies [81].

Different studies focused the attention on developing inhibitors of STAT3 DNA binding domain and STAT3 SH2 domain that would prevent dimerization and transcriptional activity of STAT3 [82-84]. Although many of these inhibitors have reached the clinical development stage, they demonstrated very limited clinical activity [85]. One issue with STAT3 SH2 inhibitors is the limited selectivity, as STAT family members share a highly structurally homologous SH2 domain. The second issue is that these small molecule inhibitors block STAT3 dimerization and only partially suppress the gene transcriptional activity of STAT3 since monomeric STAT3 protein also has transcriptional activity [86]. Lastly, monomeric STAT regulates critical mitochondrial activities, control cell shape, and motility. Properties that are not inhibited by conventional inhibitors. However, in 2001 a new and attractive approach started into small-molecule development. Crews and Deshaies laboratories reported a study based on the induction of ubiquitylation and degradation using a proteolysis-targeting chimeras (PROTACs) technology, to induce the degradation of methionine aminopeptidase-2 (MetAp-2)[87].
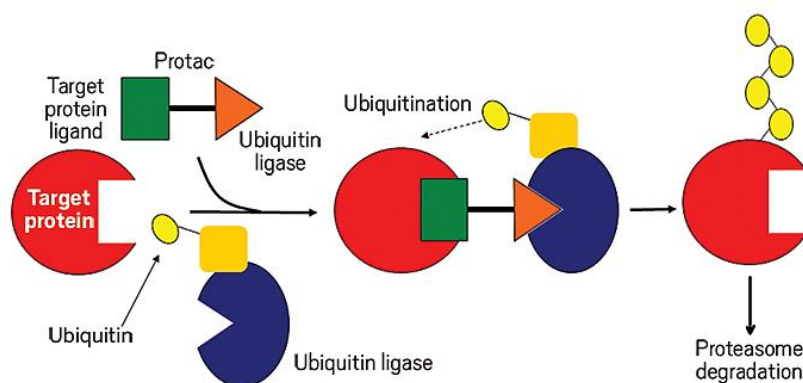
FIGURE 6– Schematic representation of bifunctional small molecules that prompt an unwanted protein to be tagged with ubiquitin, sending it to the cellular trash bin.

A PROTAC is a heterobifunctional molecule that consists of a protein of interest (POI) ligand and an E3 ubiquitin ligase (E3) recruiting ligand connected by a linker. PROTACs initiate a degradation cascade by forming a ternary complex with a POI and an E3, bringing the ubiquitination machinery nearby for subsequent POI ubiquitination. The polyubiquitinated POI is then recognized and degraded by the 26S proteasome. The 26S proteasome is part of the ubiquitin-proteasome system (UPS) which is the primary mechanism used by eukaryotic cells to regulate protein levels [88, 89]. In the last years, PROTAC strategy has begun to be more popular, and different proteins, nuclear receptors, and kinases were targets to develop new molecules [90]. Recently, Bai and colleagues showed the results of PROTAC degrader of STAT3 named SD-36. SD-36 was designed using an analog of cereblon (CRBN) ligand, lenalidomide, and the STAT3 SH2 domain inhibitor SI-109 previously developed [91].

This bifunctional molecule binds to the STAT3 SH2 domain via one functional group and CRBN via the other functional group. Once near STAT3, CRBN then forms an E3 ubiquitin ligase complex that recruits an E2 enzyme to ubiquitinate and target STAT3 for proteasomal degradation (Figure 7) [92].
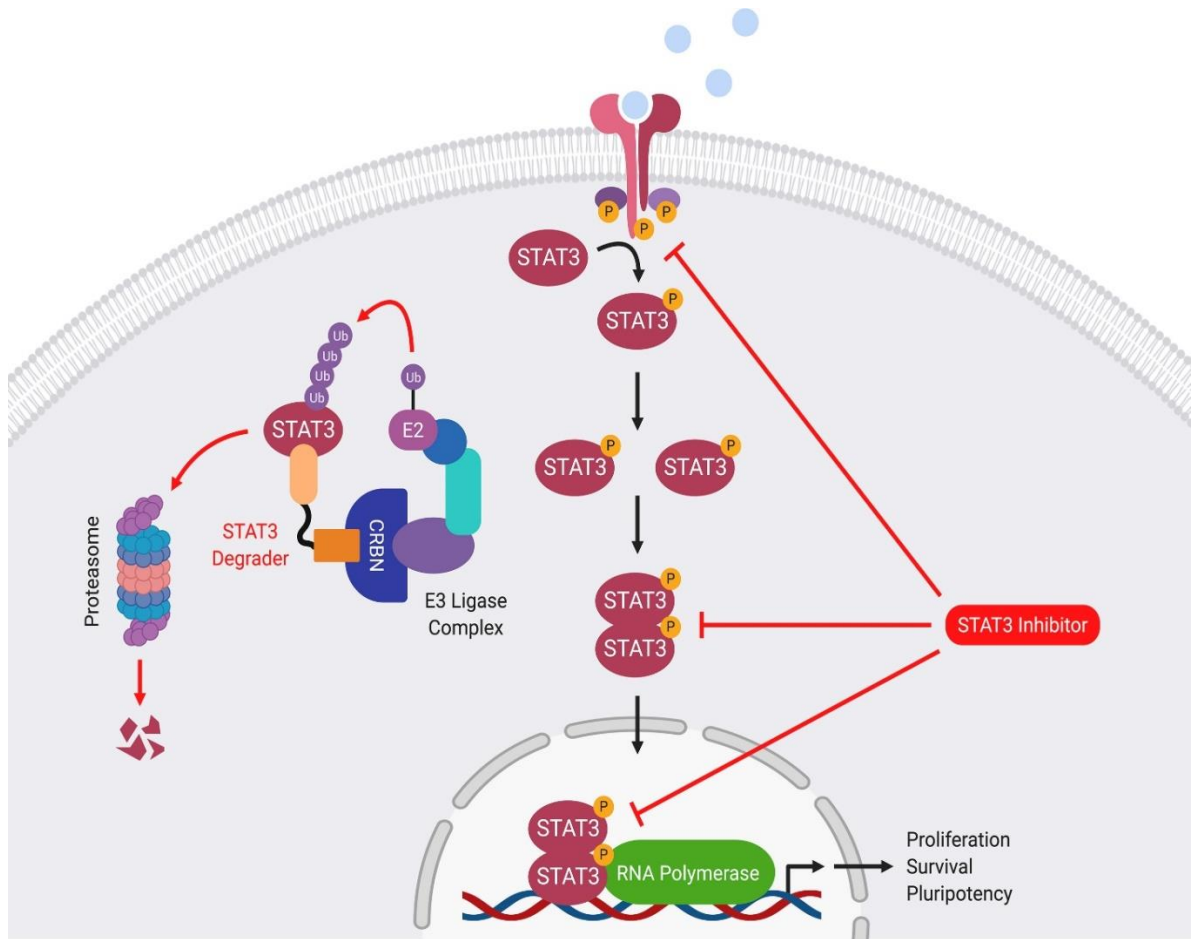
Figure 7- STAT3 Degraders Inhibit Oncogenic STAT3 Signaling by Targeting STAT3 Proteins for Proteasomal Degradation [92]. *The figure shows the different mechanisms of action of inhibitors compares to degraders. STAT3 inhibitors typically reduce STAT3 activity by blocking STAT3 tyrosine phosphorylation, STAT3 dimerization, or STAT3 DNA binding. In contrast, STAT3 degraders block STAT3 activity by triggering the degradation of the STAT3 protein.*

Bai and colleagues showing that SD-36 inhibits STAT3 dimerization, STAT3 DNA binding, STAT3-dependent reporter gene activity, STAT3 target gene expression, and STAT3-dependent proliferation in acute myeloid leukemia (AML) and ALCL cell lines. They also evaluated the therapeutic potential of SD-36 in three different mouse xenograft tumor models [91].

Whereby, perhaps these new degraders can be used to treat STAT3-driven malignancies.

Patient-Derived-Tumor-Xenograft (PDTX) model

Cancer cell lines still represent the most common models in cancer research and anticancer drug discovery in vitro. They have many advantages including the immediate accessibility to the scientific community and the reproducibility of results. The heterogeneity of the tumor environment led to developing a model that can accurately reproduce and predict in vivo drug sensitivity and response to patients, thus supporting in vitro research and cancer cell line results.

Patient-Derived-Tumor-Xenograft (PDTX) model, which was first described more than 40 years ago, may represent a valuable help for cancer research and drug discovery, not just for in vivo but also for in vitro research [93, 94].

PDTX model consists of the transplantation of a fresh human tumor specimen from a cancer patient directly into the immune-deficient mice. The histopathology of PDTX tumors closely mimics those of the donor lesions. A lot of evidence, including high fidelity in mutational status, transcriptome, histology, polymorphism, and copy number variation, also supports the notion that PDTX models remarkably resemble the pathophysiology of human tumors more closely than traditional cancer-derived xenograft (CDX) models [95].
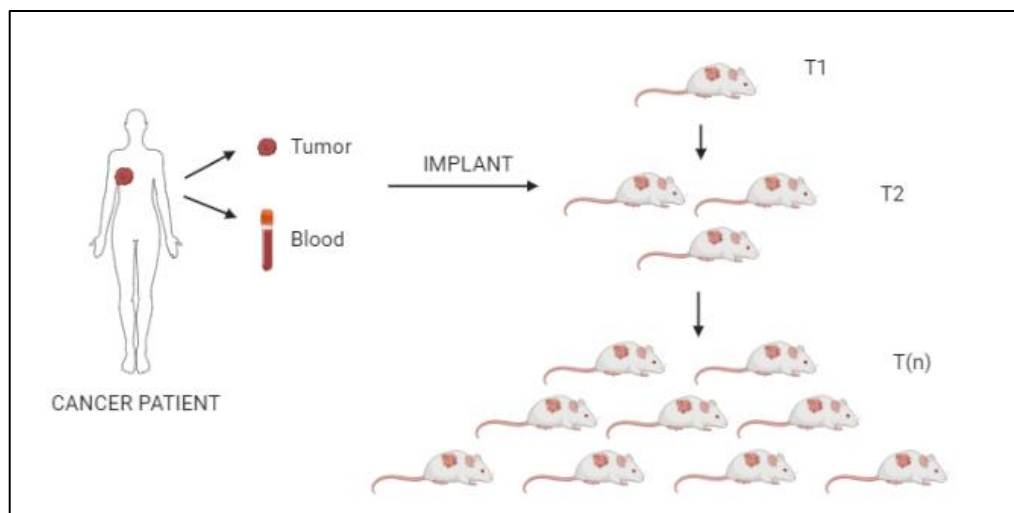

FIGURE 8– Schematic representation of PDTX generation: engraftment and expansion (Created in BioRender.com).

In the case of solid neoplasms, after sample collection, tumors are rapidly processed and tissue fragments (≈3mm3) are implanted via multiple routes, more frequently subcutaneously or orthotopically. The implantation of tissue fragments provides a rational advantage in maintaining the overall organization of the neoplastic microenvironment and ultimately preserves neoplastic niches. In the setting of liquid tumors, cancer cells are instead purified (gradient separation, etc.) and implanted (intravenous, intraperitoneal, intraspleen-liver, intrabone) in immunocompromised host animals [95]. The time of engraftment varies considerably between different cancers and among different xenograft belonging to the same tumor type. Usually, the growth takes about 2-3 months, but longer periods (>6-9 months) are not unusual. Technically, different factors can influence the rate of engraftments, such as the quality of the patient-derived material, tumor type, stage of differentiation, drug resistance, time of implant, number of cells, and routes of implantation. Perhaps the most critical variable is the selection of mouse strain. The development of RAG or NOD/SCID/ IL2Rγnull (NSG) mice represents a major achievement and has improved engraftment of primary human tumor specimens [96].

NSG mice are Scid deficient (bearing a DNA repair complex protein Prkdc mutation) resulting in profound defects in both B and T cells. They also harbor a target mutation of the gene encoding the IL2-receptor common γ chain (IL2rgnull) and the lack of signaling through IL2rg results in the functional impairment of NK cells, thus severely compromising both the innate and adaptive immunities in these animals [97]. Moreover, engineered NSG mice have emerged for specific applications (i.e. AML) and to generate more reliable humanized mice.

Inghirami's laboratory has developed a library of multiple PDTX models including 64 models from primary naïve or relapsed/refractory T-cell lymphoma (showed in table 1).

DISEASE	# SAMPLES IMPLANTED	# SAMPLES ENGRAFTED	% OF ENGRAFTMENT
ALCL	34	16	47
AITL	33	17	48.5
PTCL-NOS	32	11	34.4
MF	34	6	17.6
NK	7	3	42.8
MEITL	4	2	50
ATLL	12	3	25
Y/δ TCL	11	2	18.2
HSTC	9	1	11.1
T-PLL	8	1	12.5
TOTAL	184	62	30.71

TABLE 1 – Library of multiple PDTX models developed by Inghirami's laboratory.

For our research, we took advantage of established ALK+ and ALK- ALCL PDTX models, which were previously generated, which closely recapitulate their original primary lymphoma. We have selected those bearing genomic defects leading to the constitutive activation of the STAT3 pathway.

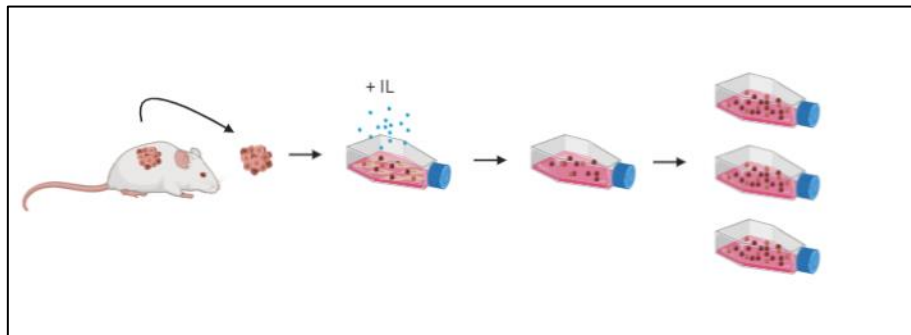The generation of PDX derived tumor cells in vitro is represented in figure 9.

FIGURE 9 – Generation of PDX derived tumor cells (Created in BioRender.com). *The generation of PDX derived tumor cells accurse after isolation of the tumor from the host animal. Subsequently, after digestion of the tumor, cells are maintained in culture medium supplemented or not of interleukins to help the growth. Fibroblasts are left to support the tumor cells growth in vitro. When the tumor cells start to grow, they were isolated from fibroblasts and maintained in culture in medium supplemented or not of interleukins and expanded.*

In particular, the experiments were performed on PDX derived tumor cells as Belli, ALK- ALCL, carrying mutations in both Jak1/Stat3; IL89, a breast implant-associated lymphoma (BIA-ALCL), with a Jak1 mutation; IL2 PTCL-NOS carrying an activating Jak1 mutation; DN03, ALK+ ALCL; IL142A, ALK- ALCL.

MATERIALS AND METHODS

Cell lines

ALK-positive ALCL human cell lines SUPM2, SU-DHL1, L82 and Karpas 299, and ALK-negative BIA-ALCL cell lines TLBR1 and TLBR2 were maintained in RPMI-1640 medium (Lonza). The medium was supplemented with 10% fetal bovine serum (FBS; Corning), 1% penicillin and streptomycin (100 IU/mL of penicillin and 100 µg/mL of streptomycin; MP Biomedicals) and 1% glutamine (200mM, Thermo Fisher Scientific). The medium for TLBR1 and TLBR2 was supplemented with recombinant human interleukin as rhIL-2 (10.000 units/ml). Cells were maintained in a 5% CO2 humidified atmosphere at 37°C.

PDX derived tumor cells

IL2 (PTCL), IL89 (BIA-ALCL), IL142A (ALK- ALCL), Belli (ALK-ALCL) and DNO3 (ALK+ ALCL) PDX derived tumor cells were maintained in RPMI-1640 medium (Lonza). Medium was supplemented with 20% FBS (Corning), 1% penicillin and streptomycin (10,000 units/mL of penicillin and 10,000 µg/mL of streptomycin; MP Biomedicals), 1% normocin (InvivoGen) and 1% glutamine (200mM, Thermo Fisher Scientific). The medium of IL2 and Belli was supplemented with recombinant human interleukin as rhIL-2 (10.000 units/ml) and rhIL-15 (10 µg/mL). Cells were maintained in a 5% CO2 humidified atmosphere at 37°C.

Human peripheral blood mononuclear cells: isolation and activation

Human peripheral blood mononuclear cells (PBMCs) from normal donors were isolated by density-gradient centrifugation using Ficoll-Paque PLUS density gradient media (GE Healthcare). PBMCs were maintained in RPMI-1640 medium (Lonza), supplemented with 10% FBS (Corning), 1% penicillin and streptomycin (100 IU/mL of penicillin and 100 µg/mL of streptomycin; MP Biomedicals),1% glutamine (200mM, Thermo Fisher Scientific). PBMCs were activated with magnetic beads conjugated to anti-human CD3 and CD28 antibodies (Dynabeads Human T- Activator CD3/CD28; Gibco), following the manufacturers' instructions. Cells were maintained in a 5% CO2 humidified atmosphere at 37°C.

Compounds

JPX-XX1 (from Janpix), A1 and N1 (from Kymera Technology) compounds were resuspended in dimethyl sulfoxide (DMSO; Sigma) and stored following the manufacturer's instructions. They were added to the cells at the indicated concentration and (different time points). DMSO was used as control.

Metabolic activity

The presence of metabolically active cells was detected by a luminescent assay. Cells were collected in a 96-well black side plate at different time points after treatments. The CellTiter-Glo Luminescent Cell Viability reagent (Promega) was added to a 1:1 cell-reagent ratio. The plate was incubated at room temperature for 10 minutes to stabilize the luminescent signal. Luminescent signal was detected by a microplate reader Biotek Synergy 4.

Caspase 3/7 activity assay

Caspase-3 and 7 activities were measured by a luminescent assay. Cells were collected in a 96-well black side plate at different time points after treatments. The Caspase-Glo 3/7 reagent (Promega) was added to a 1:1 cell-reagent ratio. The plate was incubated at room temperature for 1 hour to stabilize the luminescent signal. Luminescent signal was detected by a microplate reader Biotek Synergy 4.

Transduction

Karpas 299 cell line, Belli and IL89 PDX derived tumor cells were transduced with a lentiviral bicistronic reporter vector encoding fluorescent ubiquitination-based cell cycle indicator probes (Fucci) [98]. The Fucci lentiviral vector expresses mVenus-hGem (1/110) fused to mCherry-hCdt1(30/120) by the T2A peptide using an EF1 promoter that generates optimal levels of gene expression in progenitors. These fluorescent reporters can distinguish three cell cycle phases as G1 by red fluorescence, G1/S by yellow fluorescence, and S/G2/M by green fluorescence.

Cells were transduced at a concentration of 1×10^6 cells per milliliter at the indicated multiplicity of infection (MOI) in the same medium of culture. At 16

hours post transduction cells were washed and maintained in the same medium of culture. The mVenus and mCherry expression in transduced cells were measured 7 days post-transduction by flow cytometry.

Western Blot

Cells were washed with cold PBS, pelleted and lysed. The protein extracts were prepared using the Lysis Buffer [10 mM MgCl2, 150 mM NaCl, 1% NP40, 2% glycerol, 1 mM EDTA, 25 mM Hepes (pH 7.5)] plus protease and phosphatase inhibitors (PMSF, NaF, Na3VO4, DTT, and PIC). Total protein concentrations were measured using the Lowry assay DC Protein Assay Kit (Bio-Rad), according to the manufacturer's protocol. Equal amounts of proteins were subjected to SDS-PAGE (6-12% polyacrylamide gels), transferred to PVDF membrane (GE Healthcare) by electroblotting, and blotted with rabbit polyclonal antibody (Ab) raised against p-STAT3 (Tyr705) (1:500 dilution, Cell Signaling Technology #9131); mouse anti-STAT3 (124H6) monoclonal Ab (mAb) (1:1000 dilution, Cell Signaling Technology #9139);); rabbit anti-STAT5 mAb (1:1000 dilution, Cell Signaling Technology #94205); rabbit anti-p27 polyclonal Ab(1:1000 dilution, Cell Signaling Technology #2552); rabbit anti-Caspase3 mAb (1:1000 dilution, Cell Signaling Technology #14220); rabbit anti-ALK mAb (1:1000 dilution, Cell Signaling Technology #3633). A rabbit anti-Actin mAb (1:1000 dilution, Cell Signaling Technology #8457) and a mouse anti-GAPDH mAb (1:1000 dilution, Santa-Cruz Biotechnology sc-47724) were used as normalizers.

Flow cytometry

All cytometric analyses were performed using the FACSCanto III and Celesta instruments (BD Biosciences) and analyzed with the BDFACSDiva software and DeNovo FCS Express 7 software.

Cell Viability assay

Cells were stained with Fixable Viability Stain 700 (FVS700; BD Horizon™), according to the manufacturer's protocol. At different time points after drug treatments, cells were harvested, washed and resuspended in PBS containing

FVS700 and incubated for 15 minutes at RT in the dark. After incubation cells were washed with PBS and cell viability was analyzed at flow cytometry.

FVS700 is excited by the red laser (with an excitation maximum of 657 nm) and has a fluorescence emission maximum of 700 nm. This dye can be read out of filters commonly used for BD Horizon™ APC-R700 or Alexa Fluor® 700.

Annexin V assay

Cells were stained for annexin V using the Annexin V-PE Apoptosis Detection Kit I (BD Biosciences) according to the manufacturer's protocol. Briefly, following drug treatments at different time points, $1X10^5$ cells were pelleted and washed twice with ice-cold PBS and resuspended in 100 µl of 1X Annexin V Binding Buffer. Subsequently, 3 µl of Annexin V-PE and 3 µl of 7-Amino-Actinomycin (7-AAD) were added to the cells that were then incubated for 15 minutes at room temperature in the dark. After incubation, 100 µL of 1X Annexin V Binding Buffer was added to the stained cells and the cells analyzed by flow cytometry.

Cell Cycle assay

For analyzing the cell cycle distribution cells were stained using the Propidium Iodide Flow Cytometry Kit (Abcam) according to the manufacturer's protocol.

At different time points after drug treatments, cells were harvested and washed with PBS. The cell pellet was resuspended in 400µl cold PBS and cells were subsequently fixed with 800 µl 100% cold ethanol, overnight at 4°C. The next day fixed cells were pelleted and washed twice with cold PBS and stained in 200 µL 1X Propidium Iodide (PI) + RNase Staining Solution and incubate at 37ºC in the dark for 30 minutes. After incubation DNA content was analyzed at flow cytometry.

Transduced cells

Transduced cells were stained with Fixable Viability Stain 575V (FVS575V; BD Horizon™), according to the manufacturer's protocol. At different time points after drug treatments, cells were harvested, washed and resuspended in PBS containing FVS575V and incubated for 15 minutes at RT in the dark. After incubation cells were washed with PBS. Subsequently, cell cycle phases of viable cells were analyzed at flow cytometry.

FVS575V is excited by the Violet laser (with an excitation maximum of 396 nm) and has a fluorescence emission maximum of 572 nm. This dye can be read out of filters commonly used for BD Horizon Brilliant Violet 605 (eg, 610/20) or Pacific Orange (eg, 575/20).

Drug Screening

Cells were stained with CellTrace™ Violet Cell Proliferation Kit (Thermo Fisher Scientific), according to the manufacturer's protocol. Cells were incubated at a concentration of 1×10^6 cells per milliliter with Cell Trace (1 µM/mL). After incubation cells were washed with PBS, resuspended in the same medium of culture at the concentration of $8x10^4$/100 µL and seeded in a 96-well U-bottom plate. Subsequently, cells were treated with A1 or N1 compound (500nM) in combination with a library of 40 different drugs (1µM) and maintained in a 5% CO_2 humidified atmosphere at 37°C. After 72 hours cells were washed, resuspended in PBS and stained with PI (10 µg/mL) for 10 minutes at 4 °C. Subsequently, the drug screening was analyzed at flow cytometry by high throughput sampler (HTS; BD).

Statistical analysis

In all studies, values are expressed as mean ± standard deviation (SD). Statistical analyses were performed by unpaired Student's t-test or ANOVA for multiple comparisons, as indicated, with GraphPad Prism 8.

Differences were considered statistically significant at $p<0.05$.

AIMS OF THE THESIS

The main objective of this study is unveiling new approaches to inhibit the biological function of STAT3 in models proven to be addicted to STAT signaling. In the past, multiple approaches have been envisioned either to down-regulated the JAK-STAT3 signaling (i.e. JAK inhibitors) or to directly down-modulated the expression of STATs (RNAi, etc.). Although encouraging data were generated using these tools, many of these approaches resulted in only partial inhibition or required a long period of exposure at high (toxic) doses; liabilities which have impaired the entry of many targeting agents into the clinics. Although interesting data were generated suing RNAi, transcriptional inhibition remains largely unfeasible in vivo. To overcome these limitations, we selected two different sets of compounds derived from two different and complementary strategies, selectively targeting STAT to define their properties and their potential therapeutic activities in pre-clinical settings. The ultimate goal was to identify novel reagents that could be eventually tested in future clinical trials. For this purpose, the biological and functional characterization of new small-molecules with two different STAT3-blocking functional activity has been made. We aim to define the biological and chemical properties, the therapeutic efficacy of novel anti-STAT compounds using an array of bona fide cells and PDX models in vitro. These studies are designed to identify the best reagent to further study STAT3 mediated transcriptional regulations and underling the mechanisms leading and maintaining the neoplastic phenotype of STAT3 dependent T-cell lymphoproliferative disorders. Toward this end, we investigated:

1. Specific STAT inhibitors: these agents were selected from a large library of compounds and proven to covalently bind to STAT.

2. Specific degraders of STAT3: these reagents were discovered using an in-silico approach predicting the binding of STAT3 and known E-ligases. Chemical modifications were then implemented to improve binding affinity and selectivity.

RESULTS

1.Specific STAT inhibitors.

In collaboration with Janpix, a small firm licensed to take into the clinics a novel family of small molecule scaffolds derived from the Gunning lab at the University of Toronto, we selected two potent molecules selective binding to STAT3/5 or STAT3 only. These inhibitors were previously shown to target the SH2 domain at nanomolar concentration, suppress STAT phosphorylation, inhibit downstream transcription targets at suitable pharmacokinetic profiles. Janpix has further identified small molecules that inhibit STAT3 and STAT5 selectively as well as pan-STAT3/5 inhibitors. These agents have shown excellent efficacy in preclinical models of medulloblastoma, breast, leukemias as well as other STAT dependent cancers. JPX-XX1 and JPX-XX2 compounds were selected by the principles of molecular recognition and computational modeling, seeking to create small-molecule inhibitors of the dimerization event between two STAT proteins. In this project, we have focused on a single molecule, JPX-XX1, which displays a selective activity against STAT3. These molecules were provided to us and protected by a CDA and MTA between the Janpix and Weill Cornell Medicine.

The JPX-XX1 compound was first tested at different concentrations for 3 days. ALK+ cell cells were exposed in parallel to a selective ALK inhibitor (crizotinib) as a positive control. To improve drug efficacy, we then performed a set of experiments in which the drug, at the appropriate concentration, was refilled every 24 hours. Cells were harvested at 72 hours and evaluated. Representative data are presented in Figure 10. As depicted in Panel A, cell viability was reduced only in ALK+ ALCL (SUMP2 and SUDHL-1) cells at the highest concentration. No changes were seen in ALK- ALCL (IL89 and IL2). When we performed a metabolism assay, the data were in line with the previous cell vitality findings and by total cell counts (Figure 10C).
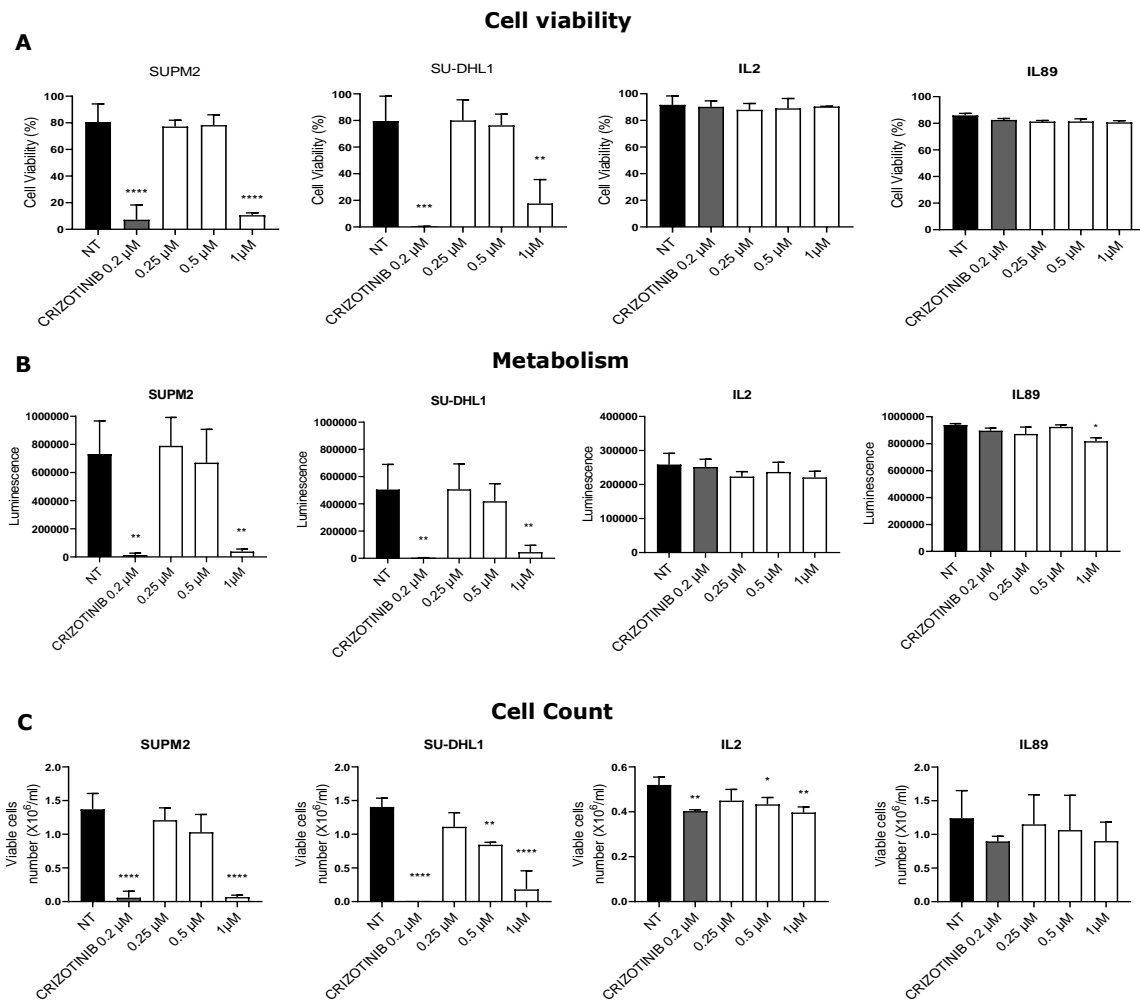
Figure 10. The JPX-XX1 compound effectively inhibits ALK+ ALCL cells. *Cells ($5x10^5$/ml) were treated with a single dose of Crizotinib (0.2 µM) at day one, while three different concentration of JPX-XX1 compound (0.25 µM, 0.5 µM and 1 µM) were used with a refilling every 24h. All the cells were left in the same media and harvested after 72h and evaluated by viability (**A**), metabolism (**B**) and count (**C**). Data represent the mean ± SD of three independent experiments. P values are for One-Way ANOVA with Dunnett's multiple comparison versus no treated cells (NT).*

Lastly, we evaluated the DNA content of the treated cells. Representative findings are depicted in Figure 11. As anticipated from the data presented in Figure 10, ALK+ ALCL cells were highly sensitive to crizotinib displaying a high rate of cell death. Only at 1µM concentration, JPX-XX1 was associated with an increased number of dead cells and a decreased fraction of cells in the S-G2 phase (Figure 11A, B), in both ALK+ ALCL and PTCL cells (Figure 11C). Interestingly, IL-89, a BIA-ALCL carrying an activating mutation of the JAK-STAT3, was not affected even at the highest dose concentrations.
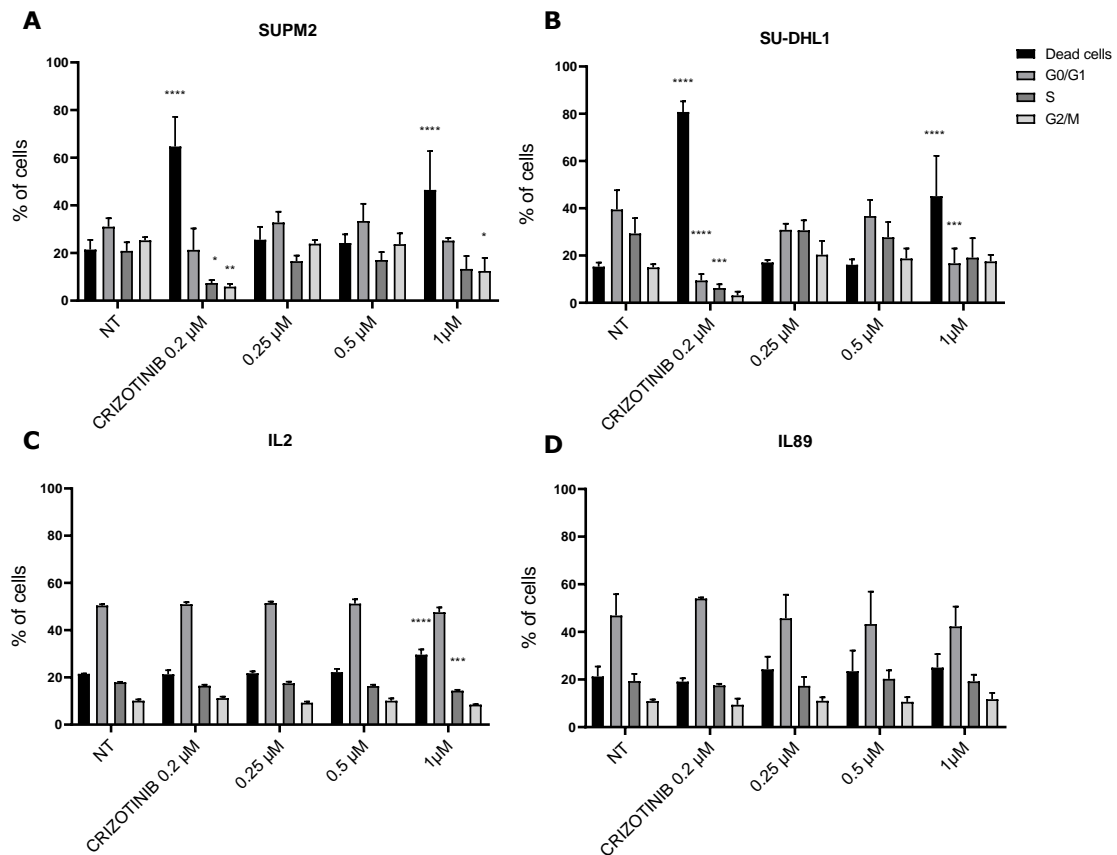
Figure 11. JPX-XX1 increases the number of dead cells when DNA content analyses are performed. *Cells (5x10⁵/ml) were treated with a single dose of Crizotinib (0.2 µM) at day one, while three different concentration of JPX-XX1 compound (0.25 µM, 0.5 µM and 1 µM) were used with a refilling every 24h. All the cells were left in the same media and harvested after 72h. Data represent the mean ± SD of three independent experiments. P values are for 2Way ANOVA with Dunnett's multiple comparison versus NT.*

Since responses were obtained at the highest concentration, we next wondered whether the effect was specific or alternately linked to general toxicity. Although the cell of origin of ALCL remains still controversial (i.e. thymocytes, Th17 cells), we thought to use peripheral blood T cells as a surrogate. Moreover, these elements could give some idea on the possible toxicity to which cells could be exposed in the blood after drug challenge. Towards this end, we isolated peripheral blood mononuclear cells from healthy donors and exposed them to increasing concentration of the drug. Since resting cells are less susceptible to toxicity, we also compared resting versus activated T-cells. Activated cells were generated engaging CD3+ cells to coated beads conjugated to anti-human CD3 and CD28 antibodies for 72 hours. As depicted in Figure 12A, engagement of CD3 + second signals was effective. Exposure to the highest concentration was associated with a significant cell loss (Figure 12B, C) likely due to increased cell

death as suggested by the Annexin staining (Figure 12D, E). These data were supported by the ATPlite readouts of activated cells, meanwhile resting cells did not provide useful information in this assay (Figure 12F, G).
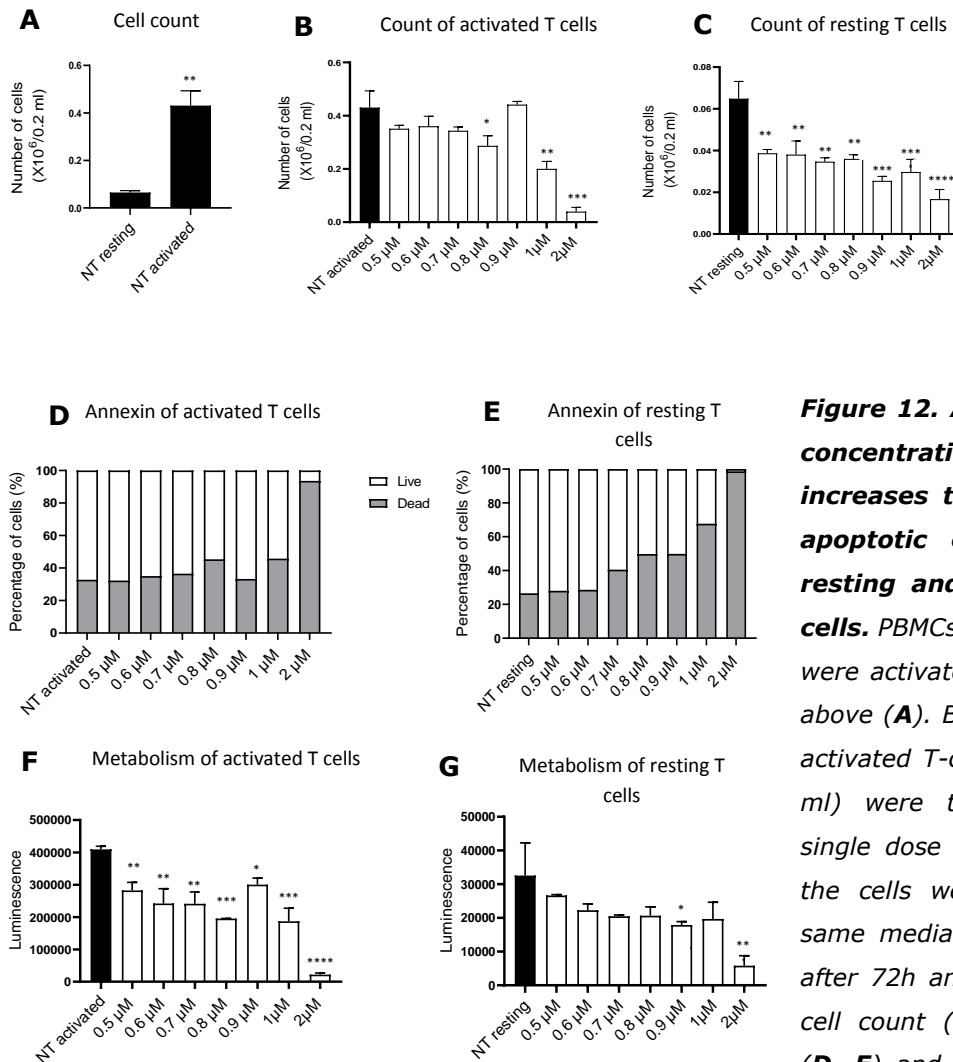

Figure 12. At the highest concentration JPX-XX1 increases the number of apoptotic cells in both resting and activated T-cells. *PBMCs from the donor were activated as described above (**A**). Both resting and activated T-cells ($8X10^4/0.2$ ml) were treated with a single dose of JPX-XX1. All the cells were left in the same media and harvested after 72h and evaluated by cell count (**B, C**), viability (**D, E**) and metabolism (**F, G**). Data represent a single experiment. The duplicate was available just for count and metabolic assay. P values are for One-Way ANOVA with Dunnett's multiple comparison versus no treated cells (NT). No treated activated cells (NT activated) and no treated resting cells (NT resting) were used as controls for activated and resting treated cells respectively.*

2.Specific degraders of STAT3

Degraders exploit the intracellular ubiquitin-proteasome system to selectively eliminate target proteins. Two selected STAT3 compounds were provided to us by Kymera Therapeutic under a specific CDA and MTA. Kymera has developed a discovery engine that is fueled by unique algorithms and sophisticated workflows. Using a holistic approach to drug discovery and development, Kymera can fine-tune the potency of drug candidates based not only on their drug-like properties but also on their relationship with target properties and downstream PK/PD effects. Targeted protein degradation using this technology is emerging as a novel therapeutic method to address diseases driven by the aberrant expression of a disease-causing protein. Degrader molecules are bifunctional small molecules that simultaneously bind a target protein and one of the E3-ubiquitin ligases, thus causing ubiquitination and degradation of the target protein by the proteasome. Like small molecules, degrader molecules possess good tissue distribution and the ability to target intracellular proteins, even in the nuclear compartment. To test these tow STAT3 compounds, we have selected conventional ALK + ALCL cell lines (L82 and Karpas 299) and ALK-ALCL PDTX models (IL89 and Belli).

A1 and N1 degraders were first tested at different concentrations in a time-course experiment. Serial dilutions of the drugs were performed to obtain a wide concentration curve. Cells were exposed for 3 days to a single administration of the compounds, and every 24 hours, cells were harvested and evaluated by metabolic assay (Figures 13,14,15 and 16). As depicted in Figures 13 and 15, ALK+ ALCL cell lines were highly sensitive to both degraders, even at lower concentrations, with a reduction of metabolic activity at 48 hours. No changes were seen in IL89, while Belli showed a more significant sensitivity to A1 degrader after longer exposures (Figure 14C). Remarkably, as for JPX-XX1, IL-89 was resistant.
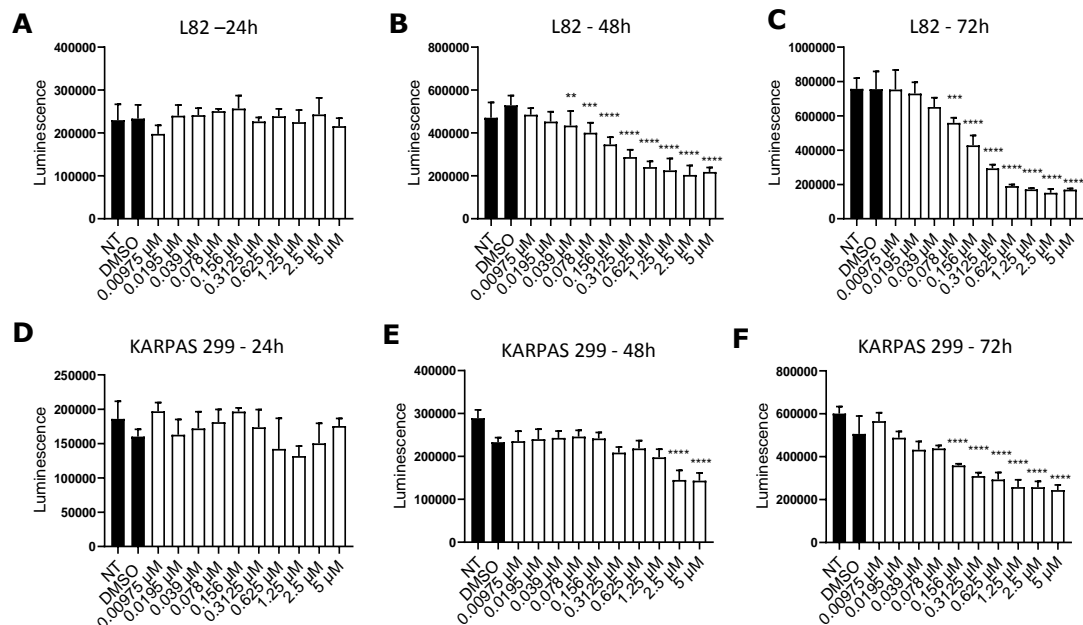
Figure 13. The A1 degrader starts to reduce the metabolic activity of ALK+ ALCL cells after 48h. *Cells (1X10^4/0.1 ml) were seeded in a 96-well plate and treated with a serial dilution of A1 degrader, with a single administration. Cells were left in the same media and harvested after 24h (**A, D**), 48h (**B, E**) and 72h (**C, F**), and evaluated by metabolic assay. Data represent the mean ± SD of four experiments. P values are for One-Way ANOVA with Dunnett's multiple comparison versus DMSO.*
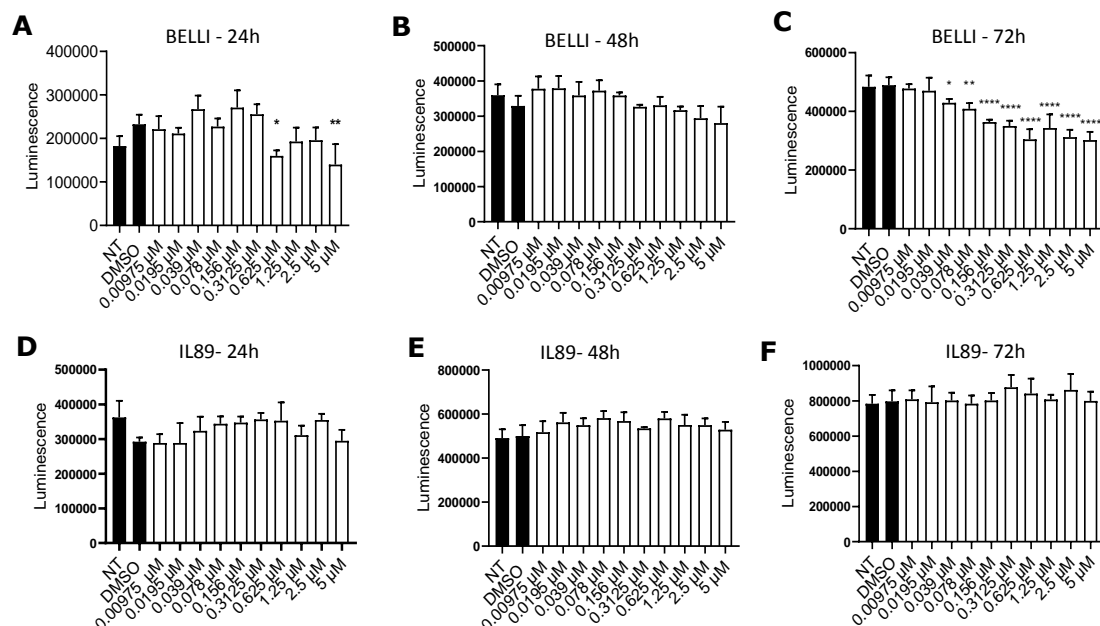

Figure 14. The A1 degrader reduces the metabolic activity of Belli. *Cells (1X10^4/0.2 ml) were seeded in a 96-well plate and treated with a serial dilution of A1 degrader, with a single administration. Cells were left in the same media and harvested after 24h (**A, D**), 48h (**B, E**) and 72h (**C, F**), and evaluated by metabolic assay. Data represent the mean ± SD of four experiments. P values are for One-Way ANOVA with Dunnett's multiple comparison versus DMSO.*
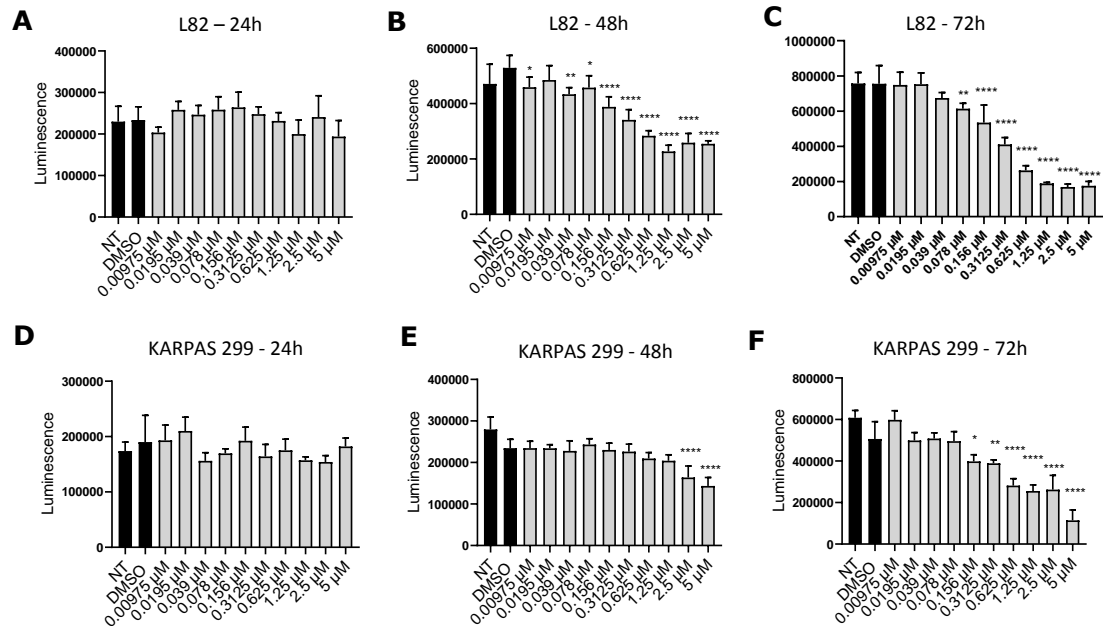
Figure 15. The N1 degrader starts to reduce the metabolic activity of ALK+ ALCL cells after 48h. *Cells (1X10^4/0.1 ml) were seeded in a 96-well plate and treated with a serial dilution of N1 degrader, with a single administration. Cells were left in the same media and harvested after 24h (**A, D**), 48h (**B, E**) and 72h (**C, F**), and evaluated by metabolic assay. Data represent the mean ± SD of four experiments. P values are for One-Way ANOVA with Dunnett's multiple comparison versus DMSO.*
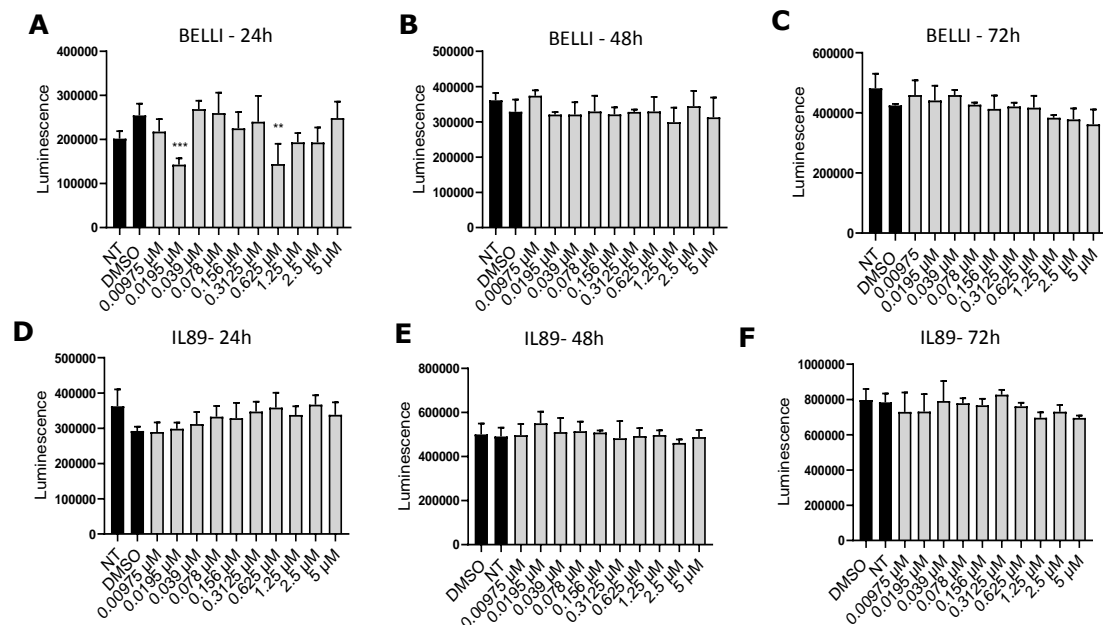

Figure 16. The N1 degrader is not effective to reduce the metabolic activity of ALK- ALCL cells. *Cells (1X10^4/0.1 ml) were seeded in a 96-well plate and treated with a serial dilution of N1 degrader, with a single administration. Cells were left in the same media and harvested after 24h (**A, D**), 48h (**B, E**) and 72h (**C, F**), and evaluated by metabolic assay. Data represent the mean ± SD of four experiments. P values are for One-Way ANOVA with Dunnett's multiple comparison versus DMSO.*

Next, to validate the efficiency of the degraders, we performed a series of western blot analyses. In these experiments, we treated the target cells with three different concentrations of the degraders, and we used the DMSO as a control vehicle. Cells were harvested and lysed (24h), and proteins were used for western blot analysis to detect phospho-STAT3, total STAT3, and actin as a control (Figure 17). Loss of STAT3 was documented in each cell line, although the degree and the kinetics were quite different among all of them. Notably, ALK+ ALCL cell lines showed a significant loss which occurs with the lowest concentrations (Figure 17A, B), with both degraders. Conversely, ALK- ALCL were more resistant and loss of STAT3 was documented at the highest concentrations (Figure 17C and D). Interestingly Belli and IL-89 display a selective sensitivity to these two degraders, suggesting that specific E-ligases may play a different role in these cells.
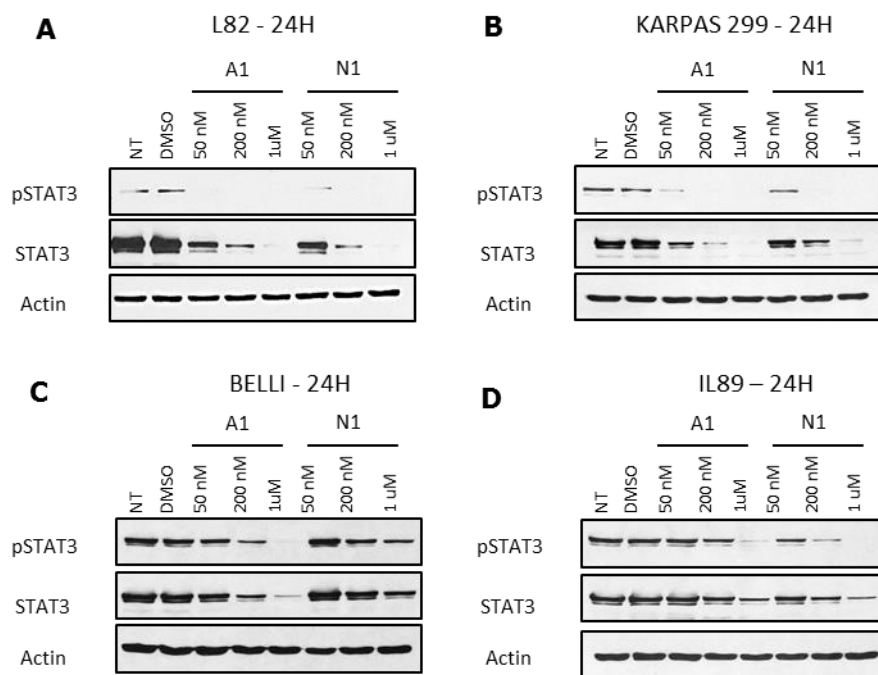

Figure 17. The loss of p-STAT3 and total STAT3 after 24 hours of treatment with A1 and N1 degraders. *Cells (2X10^5/ml) were treated with three different concentrations of A1 and N1 degraders. DMSO was used as control. After 24h of the single administration of the drugs, cells were harvested and lysed. Proteins were separated by electrophoresis, transferred to the PVDF membrane, and incubated with antibodies against p-STAT3, total STAT3, and actin as a control.*

Next, we performed a set of experiments designed to dissect further the kinetics and drug efficiency over time. Towards this end, we first exposed the cells to

different concentrations of A1 or N1 for a longer time (> 72h). At day three the cells were randomized two different arms: half cells were left in the same condition without a drug refilling; meanwhile the remaining cells were cultured with new media and new drugs. In both cases, cells were harvested every 24h and evaluated by caspase 3/7 activity assay (Figure 18). To perform these experiments, we matched the best degrader for each cell line (Figure 17).

As depicted in Figure 18, at the highest concentration we observed an increased cell death rate as documented by the Caspase assay. Remarkably, when the cells were refed, cell viability was apparently restored. Data which could be linked to the decreased number of viable cells at 96hr pre-refilling (Figure 18). To supports these data also we performed time-course assays as well as cell count (Figure 19) and Annexin V (Figure 20). Overall these data demonstrated that there was an increased cell death overtime and dose-response in both ALK+ ALCL and Belli. Remarkably IL-89 was refractory.
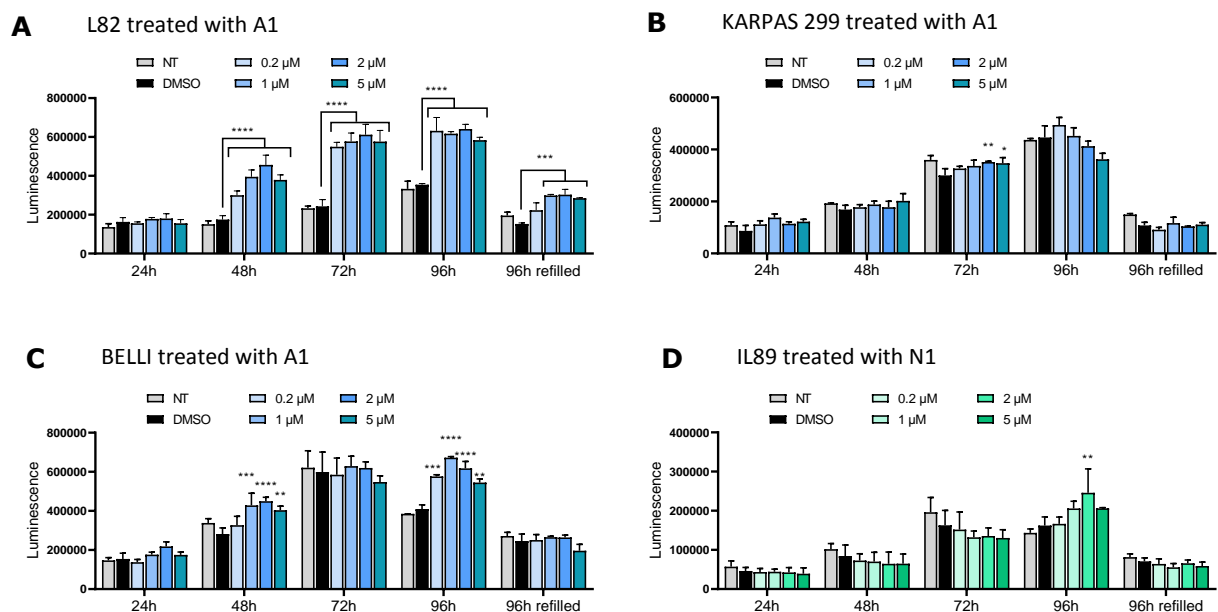

Figure 18. Caspase 3 and 7 activities increased for L82 and Belli after treatment with A1. *Cells ($2X10^5$/ml) were treated with four different concentrations of degraders, with a single administration at day 0. L82 (**A**), Karpas 299 (**B**) and Belli (**C**) cells were treated with the degrader A1, while N1 was used to treat IL89 (**D**). After 72h of treatment cells were split in two: half cells were left in the same media without refilling of the drugs; the other half cells were washed with PBS, counted, restored at the same condition as day 0 ($2X10^5$ cells per ml, refilled of new media and new drugs). All the cells, refilled or not at day 3, were collected every 24h and evaluated by caspase 3/7 activity assay. Data represent the mean ± SD of three experiments. P values are for 2Way ANOVA with Dunnett's multiple comparison versus DMSO.*
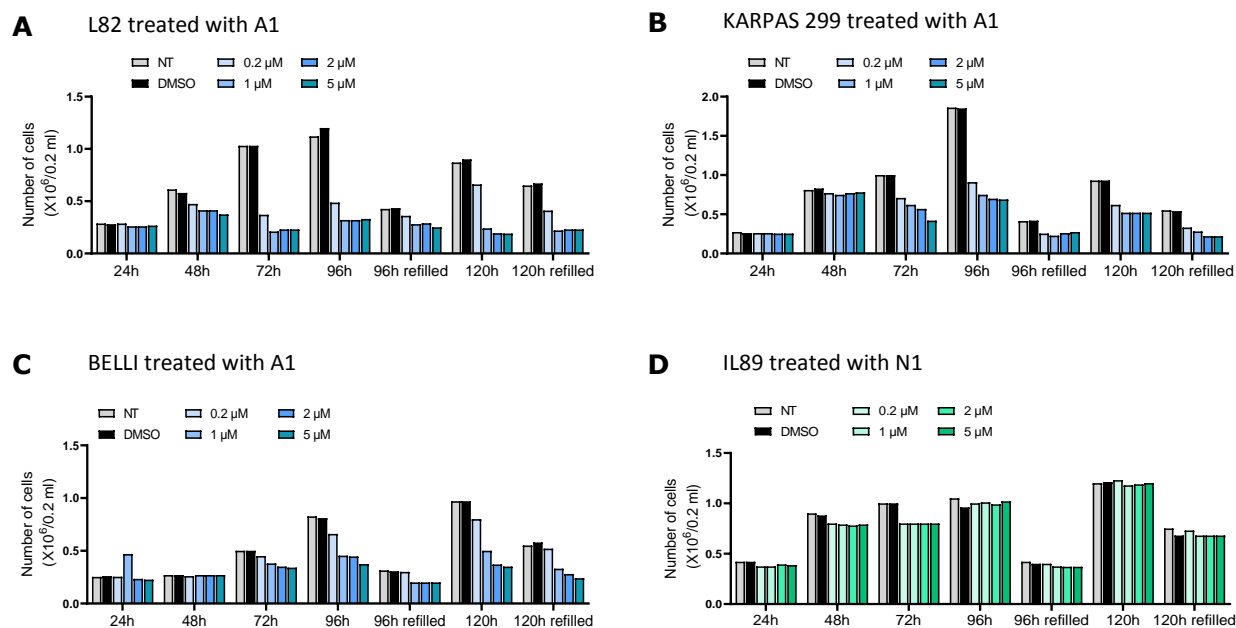
Figure 19. A1 degrader reduces the number of L82, Karpas 299 and Belli with or without refilling. Cells ($2X10^5$/ml) were treated with four different concentrations of degraders, with a single administration at day 0. L82 (**A**), Karpas 299 (**B**) and Belli (**C**) cells were treated with the degrader A1, while N1 was used to treat IL89 (**D**). DMSO was used as control. After 72h of treatment cells were split in two: half cells were left in the same media without refilling of the drugs; the other half cells were washed with PBS, counted, restored at the same condition as day 0 ($2X10^5$ cells per ml, refilled of new media and new drugs). All the cells, refilled or not at day 3, were collected every 24h and counted.
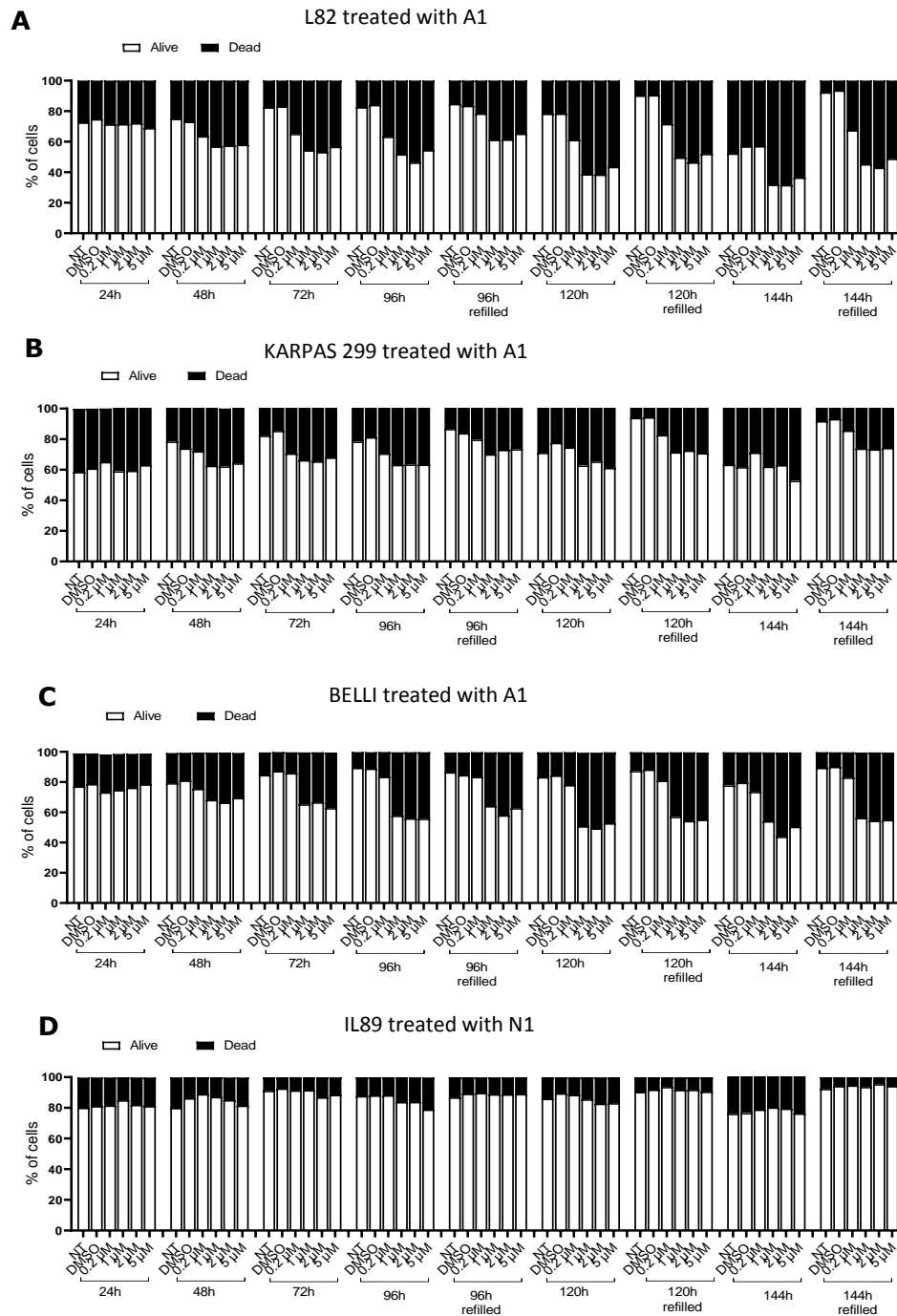
Figure 20. A1 degrader increases the number of apoptotic cells of L82, Karpas 299 and Belli in a time course experiment. *Cells (2X10^{5}/ml) were treated with four different concentrations of degraders, with a single administration at day 0. L82 (**A**), Karpas 299 (**B**) and Belli (**C**) cells were treated with the degrader A1, while N1 was used to treat IL89 (**D**). DMSO was used as control. After 72h of treatment cells were split in two: half cells were left in the same media without refilling of the drugs; the other half cells were washed with PBS, counted, restored at the same condition as day 0 (2X10^{5} cells per ml, refilled of new media and new drugs). All the cells, refilled or not at day 3, were collected every 24h and counted.*

To interpret these data and gain some insights into the mechanism of action, we performed a new set of western blot analyses. Cells were exposed to drugs and harvested at 96h or 144h. Cells were lysed, and proteins were used for western blot analysis to detect total STAT3 and actin or GAPDH as a control (Figure 21). In these experimental conditions, the protein expression of total STAT3 significantly reduced even at the lowest concentrations and virtually no signals were detectable at longer exposures in samples treated with >1µM. Remarkably both NPM-ALK and STAT5 signals were unchanged all conditions.

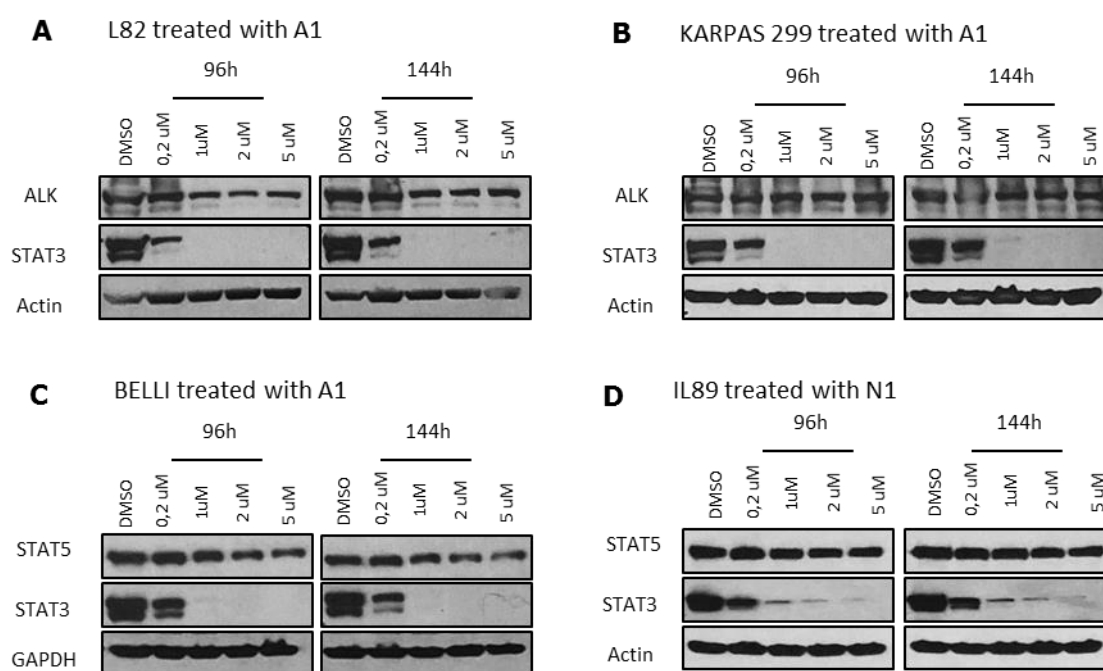*Figure 21. The loss of total STAT3 after long exposure of treatment with A1 or N1 degraders.* Cells (2X10^5/ml) were treated with four different concentrations of degraders. L82 (*A*), Karpas 299 (*B*) and Belli (*C*) cells were treated with the degrader A1, while N1 was used to treat IL89 (*D*). DMSO was used as control. After 96h and 144h of the single administration of the drugs, cells were harvested and lysed. Proteins were separated by electrophoresis, transferred to the PVDF membrane and incubated with antibodies against, total STAT3, ALK, total STAT5, and actin or GAPDH as a control.

Next, we extended these analyses to a large set of cell lines including both ALK- and ALK+ ALCL, BIA-ALCL and PTCL-NOS. These included three ALCL PDTX models as IL2 PTCL-NOS, DN03 ALK+ ALCL and, IL142A ALK- ALCL; and on

TLBR1 and TLBR2, BIA-ALCLs ALK-. Cells were exposed to different concentrations of A1 and N1 degraders and harvested after 24h exposure. These data confirmed our previous findings and demonstrated a unique cell line sensitive to individual compounds. i.e. IL2, DNO3, and TLBR1 cells were more sensitive to the A1 compound, while IL142A showed more affinity for N1 (Figure 22). Notably, TLBR1 and DN03 cells appear to be less sensitive and TLBR2 was resistant to both degraders (Figure 22F).
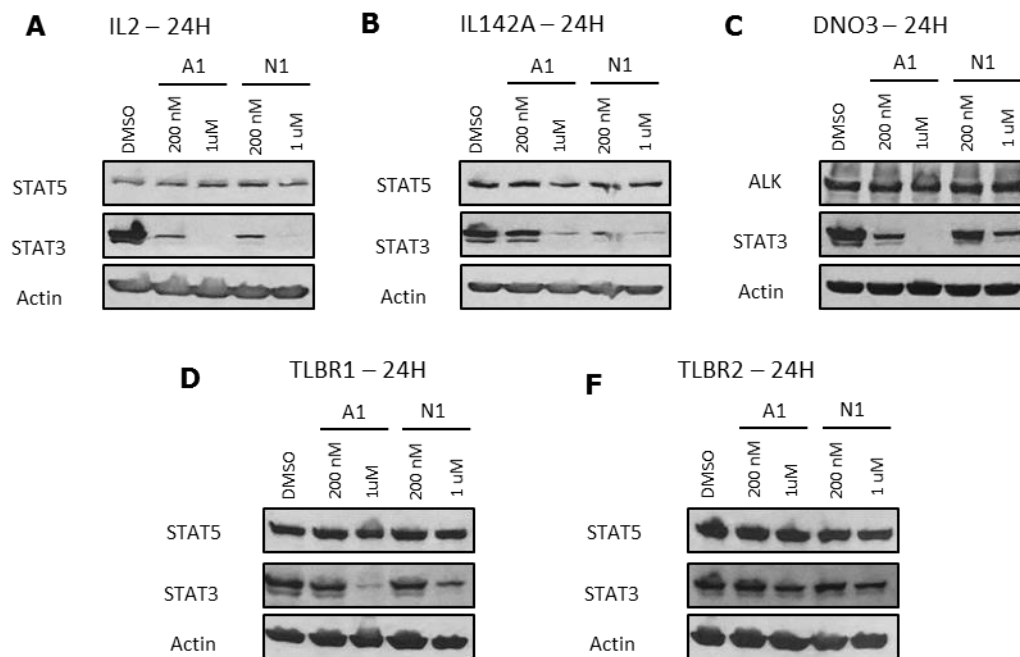

Figure 22. IL2, IL142A, DNO3, and TLBR1 cells lose STAT3 when treated with the degraders. *Cells ($2X10^5$/ml) were treated with two different concentrations of A1 and N1 degraders. DMSO was used as control. After 24h of the single administration of the drugs, cells were harvested and lysed. Proteins were separated by electrophoresis, transferred to the PVDF membrane and incubated with antibodies against, total STAT3, ALK, total STAT5, and actin as a control.*

Previous data, from our group and other investigators, have shown that the loss of STAT3 is associated with a rapid cell cycle arrest followed by sensitive cell line apoptosis. To investigate possible cell cycle changes after drug exposure, we took advantage of a new cell cycle reporter. This vector allows the detection of cells in different cell cycle phases based on two fluorescent reporter probes. Karpas 299, Belli, and IL89 cells were first transduced with concentrated lentiviral preparations and followed over time. Indeed, transduced Fucci

lentiviral vector cells express mVenus-hGem (1/110) fused to mCherry-hCdt1(30/120), which can distinguish three cell cycle phases as G1 by red fluorescence, G1/S by yellow fluorescence, and S/G2/M by green fluorescence. Figure 23A shows an example of the gating strategy of transduced cells before and after the treatment of the degraders. The double negative (untransduced, UT) cells were excluded from the analysis. Cells were treated with different concentrations of the degraders, and every 24h cells were harvested, and viable cells were evaluated by flow cytometry. The treatment with A1 degrader of both transduced Karpas 299 and Belli cells increased the fraction of cells in the G1-arrest phase at a different time point, with a consequently decreased fraction of cells in the S-G2 phase (Figure 23 panel B and C)
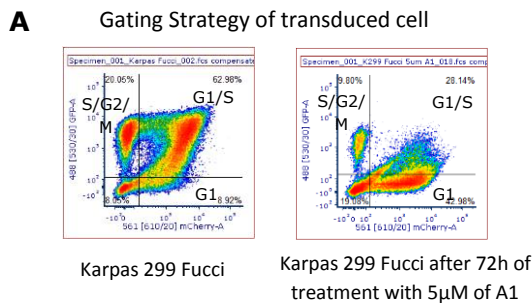

A   Gating Strategy of transduced cell

Karpas 299 Fucci

Karpas 299 Fucci after 72h of treatment with 5µM of A1

Figure 23. Karpas 299 and Belli cells transduced with Fucci vector are in the G1-arrest phase after treatment with A1 degrader. Cells ($1X10^6$/ml) were transduced with the Fucci vector at the MOI of 30 (B, C) or the MOI of 50 (D). The mVenus and mCherry expression in transduced cells were measured 7 days post-transduction by flow cytometry (A). Cells were treated with four different concentrations of A1 (B, C) or N1 (D) degraders. Every 24h cells were harvested, and viable cells were evaluated by flow cytometry. UT cells were excluded by the analysis. DMSO was used as control.

B   KARPAS 299 treated with A1 degrader
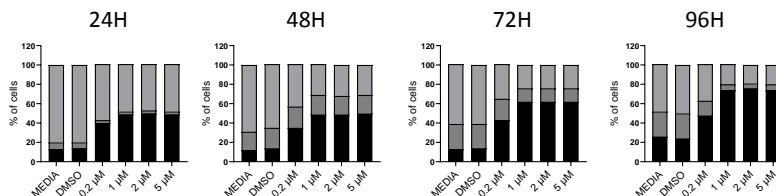
C   BELLI treated with A1 degrader
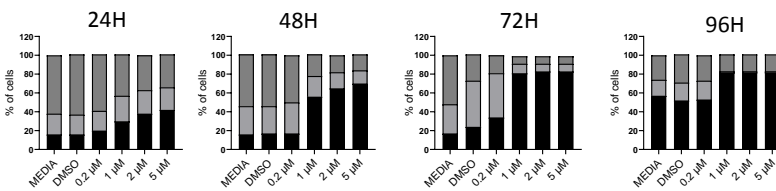
D   IL89 treated with N1 degrader

Lastly, we tested whether we could find a synergism with a battery of compounds known to target selective proteins/pathways. This was achieved using an agnostic drug screening assay, testing the A1 and N1 degraders in combination with a library of 40 different drugs. We selected the L82 cell line, which is sensitive to the activity of both degraders. Cells were first stained with Cell Trace Violet dye, then seeded into 96-well plates and charged with each drug from the library, with or without A1 or N1. DMSO was used as a vehicle. After 72h, cells were stained with PI and the number of apoptotic cells was evaluated by flow cytometry. As depicted in Figure 24, no significant changes were seen between L82 treated with the library alone or in combination with one of the degraders. Although these data are very preliminary, they prove that this platform can be used to study drug synergism using a semiautomated high throughput approach. We are currently performing additional tests to investigate new combinations, multiple PDX lines, and different readouts.

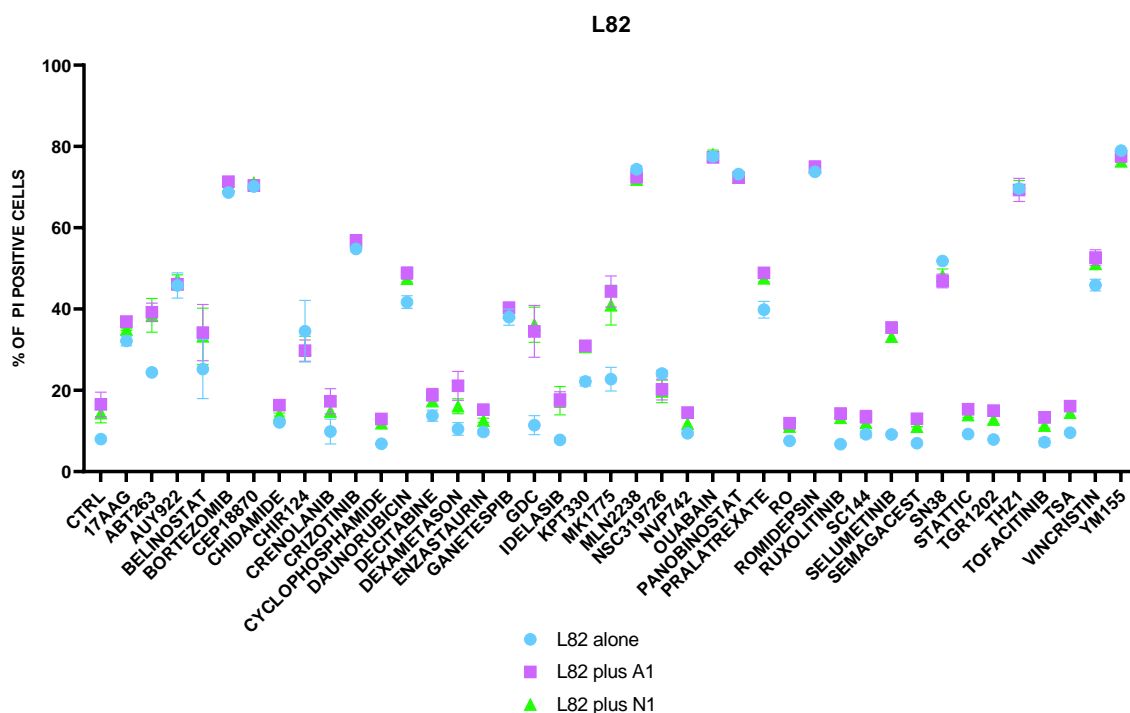**Figure 24. Degraders in combination with the drug library do not increase the number of apoptotic cells.** *Cells (8X10^4/100 μL) were stained with Cell Trace Violet dye, treated with 1 μM of each drug form the library, in combination or not with 1 μM of A1 or N1 degrader. After 72h cells were stained with PI and the number of positive cells was evaluated by flow cytometry.*

DISCUSSION

PTCLs are rare and aggressive types of NHL, characterized by low survival, poor outcomes, and a high rate of relapses [99]. This clinical scenario has been mainly related to the limited knowledge of the driving mechanisms of these neoplasms. However, new molecular and functional findings have recently fostered the design and implementation of innovative therapeutic protocols and the usage of promising targeted therapies [100]. In the last decade, it has become evident that a subset of hematologic malignancies displays the constitutive activation of STAT3, drawing attention to its role as a therapeutic target. Among them, lymphomas have been shown to be dependent on the constitution activation of STAT3 signaling, driven either via ALK chimeras or by the somatic activating mutation of JAK1/STAT3. [38,80].

Here, we focused on two pharmacological approaches to modulate the activity of STAT3 aiming to test in the preclinical setting new molecules that could be exported into the clinics.

Our data demonstrate that ALK + ALCL cells are selectively sensitive to JPX-XX1. Decreased metabolic rates and impaired viability were not observed only in ALK + ALCL cells, but also in PTCL models, leading to activating mutation of JAK or STAT3. In contrast, a BIA-ALCL PDX (IL89) tumor model, also carrying an activating JAK mutation, was extraordinarily resistant. Data suggesting that a genomic footprint may not be totally predictive of the response. When we explored the potential toxicity of these compounds, we discovered some degree of toxicity in peripheral blood mononuclear cells at rest or activated at very high concentrations (> 2μM), suggesting that a therapeutic window could potentially be reached. Indeed, remarkable data were seen with two new highly selective STAT3 degraders These molecules were proven not only to be highly specific but also effective and capably to maintain low STAT3 protein levels for a long period. More remarkably, their efficacy was achievable at very low concentration (to 50 nM to 1μM), and more impressive was the sustained effect of the single dose during the time. These findings were observed with the large majority of the models with one single exception, IL89, a BIA-ALCL, which was frankly refractory. Interestingly, we found that the therapeutic efficacy of the degraders was linked to selective E-ligase expressed in each cell line, suggesting that

individual lymphoma should be tested upfront to established which E-ligase may be explored and those which degrader may be used. A strategy that can be executed likely using a limited number of biomarkers. Collectively, the properties of these compounds anticipate that it may be possible to establish the broad therapeutic window and the possibility to reach therapeutic efficacy with a limited amount of drugs and low overtime exposure, a scenario that may be associate with mild or no toxicity. Lastly, the exquisite specificity of these molecules makes them ideal drugs for targeting STAT3 dependent processes. These unique features, however, could also represent liabilities, considering that some neoplasms may be addicted to both STAT3 and STAT5 and/or compensatory circuitry (i.e. activation of alternative STAT5 pathways) may occur in STAT5 addicted lymphoma after STAT3 inhibition. In this latter scenario, someone could anticipate that responses may be delayed/tempered, and a possible combination of degraders target different molecules may be necessary.

Mechanistically, it is known that STAT3 regulates a plethora of molecules via both canonical and non-canonical pathways. However, the precise mechanisms which operate of each tumor are still largely unclear. Our data have confirmed that the loss/inhibition of STAT3 can lead first to cell cycle arrest followed over time by cell death. Nevertheless, the rate of apoptotic cells was relatively low and quite variable in different models; data in line with those generated in patients with myeloproliferative disorders treated with JAK inhibitors, suggesting that prolonged exposure may be required to reach significant results. Based on these findings, we have envisioned to perform an agnostic drug screening searching for possible combinations. We believe that this approach may provide new avenues to define synergist activities particularly in the setting of ALK- ALCL or JAK/STAT3 PTCL.

In sum, we believe that the entry of degraders in clinical settings is offering new and unpredictable opportunities. Indeed, these molecules may overcome the most difficult task of modern pharmacology, i.e. targeting transcription factors. Their impressive selectively, the prolonged efficacy and the potency of these new compounds are astonishing features, rarely achievable using conventional discovery program.

REFERENCES

1.   Vose, J., J. Armitage, and D. Weisenburger, International peripheral T-cell and natural killer/T-cell lymphoma study: pathology findings and clinical outcomes. J Clin Oncol, 2008. 26(25): p. 4124-30.

2.   Swerdlow, S.H., International Agency for Research on Cancer., and W.H. Organization., WHO classification of tumours of haematopoietic and lymphoid tissues. 4th ed. World Health Organization classification of tumours. 2008, Lyon, France: International Agency for Research on Cancer. 439 p.

3.   Stein, H., et al., The expression of the Hodgkin's disease associated antigen Ki-1 in reactive and neoplastic lymphoid tissue: evidence that Reed-Sternberg cells and histiocytic malignancies are derived from activated lymphoid cells. Blood, 1985. 66(4): p. 848-58.

4.   Fischer, P., et al., A Ki-1 (CD30)-positive human cell line (Karpas 299) established from a high-grade non-Hodgkin's lymphoma, showing a 2;5 translocation and rearrangement of the T-cell receptor beta-chain gene. Blood, 1988. 72(1): p. 234-40.

5.   Rimokh, R., et al., A translocation involving a specific breakpoint (q35) on chromosome 5 is characteristic of anaplastic large cell lymphoma ('Ki-1 lymphoma'). Br J Haematol, 1989. 71(1): p. 31-6.

6.   Mason, D.Y., et al., CD30-positive large cell lymphomas ('Ki-1 lymphoma') are associated with a chromosomal translocation involving 5q35. Br J Haematol, 1990. 74(2): p. 161-8.

7.   Bitter, M.A., et al., Morphology in Ki-1(CD30)-positive non-Hodgkin's lymphoma is correlated with clinical features and the presence of a unique chromosomal abnormality, t(2;5)(p23;q35). Am J Surg Pathol, 1990. 14(4): p. 305-16.

8.   Morris, S.W., et al., Fusion of a kinase gene, ALK, to a nucleolar protein gene, NPM, in non-Hodgkin's lymphoma. Science, 1994. 263(5151): p. 1281-4.

9.   Chiarle, R., et al., The anaplastic lymphoma kinase in the pathogenesis of cancer. Nat Rev Cancer, 2008. 8(1): p. 11-23.

10. Stein, H., et al., CD30(+) anaplastic large cell lymphoma: a review of its histopathologic, genetic, and clinical features. Blood, 2000. 96(12): p. 3681-95.

11. Savage, K.J., et al., ALK- anaplastic large-cell lymphoma is clinically and immunophenotypically different from both ALK+ ALCL and peripheral T-cell lymphoma, not otherwise specified: report from the International Peripheral T-Cell Lymphoma Project. Blood, 2008. 111(12): p. 5496-504.

12. Benharroch, D., et al., ALK-positive lymphoma: a single disease with a broad spectrum of morphology. Blood, 1998. 91(6): p. 2076-84.

13. Jaffe, E.S., Anaplastic large cell lymphoma: the shifting sands of diagnostic hematopathology. Mod Pathol, 2001. 14(3): p. 219-28.

14. Kesler, M.V., et al., Anaplastic large cell lymphoma: a flow cytometric analysis of 29 cases. Am J Clin Pathol, 2007. 128(2): p. 314-22.

15. Wellmann, A., et al., Analysis of the t(2;5)(p23;q35) translocation by reverse transcription-polymerase chain reaction in CD30+ anaplastic large-cell lymphomas, in other non-Hodgkin's lymphomas of T-cell phenotype, and in Hodgkin's disease. Blood, 1995. 86(6): p. 2321-8.

16. Iwahara, T., et al., Molecular characterization of ALK, a receptor tyrosine kinase expressed specifically in the nervous system. Oncogene, 1997. 14(4): p. 439-49.

17. Morris, S.W., et al., ALK, the chromosome 2 gene locus altered by the t(2;5) in non-Hodgkin's lymphoma, encodes a novel neural receptor tyrosine kinase that is highly related to leukocyte tyrosine kinase (LTK). Oncogene, 1997. 14(18): p. 2175-88.

18. Stoica, G.E., et al., Identification of anaplastic lymphoma kinase as a receptor for the growth factor pleiotrophin. J Biol Chem, 2001. 276(20): p. 16772-9.

19. Stoica, G.E., et al., Midkine binds to anaplastic lymphoma kinase (ALK) and acts as a growth factor for different cell types. J Biol Chem, 2002. 277(39): p. 35990-8.

20. Webb, T.R., et al., Anaplastic lymphoma kinase: role in cancer pathogenesis and small-molecule inhibitor development for therapy. Expert Rev Anticancer Ther, 2009. 9(3): p. 331-56.

21.   Shi, X.L., X.W. Tang, and D.P. Wu, Research progresses in the pathogenesis of anaplastic large cell lymphoma. Chin J Cancer, 2011. 30(6): p. 392-9.

22.   Lamant, L., et al., Expression of the ALK tyrosine kinase gene in neuroblastoma. Am J Pathol, 2000. 156(5): p. 1711-21.

23.   Miyake, I., et al., Activation of anaplastic lymphoma kinase is responsible for hyperphosphorylation of ShcC in neuroblastoma cell lines. Oncogene, 2002. 21(38): p. 5823-34.

24.   Powers, C., et al., Pleiotrophin signaling through anaplastic lymphoma kinase is rate-limiting for glioblastoma growth. J Biol Chem, 2002. 277(16): p. 14153-8.

25.   Grzelinski, M., et al., Ribozyme-targeting reveals the rate-limiting role of pleiotrophin in glioblastoma. Int J Cancer, 2005. 117(6): p. 942-51.

26.   Dirks, W.G., et al., Expression and functional analysis of the anaplastic lymphoma kinase (ALK) gene in tumor cell lines. Int J Cancer, 2002. 100(1): p. 49-56.

27.   Pulford, K., et al., Detection of anaplastic lymphoma kinase (ALK) and nucleolar protein nucleophosmin (NPM)-ALK proteins in normal and neoplastic cells with the monoclonal antibody ALK1. Blood, 1997. 89(4): p. 1394-404.

28.   Falini, B., et al., ALK expression defines a distinct group of T/null lymphomas ("ALK lymphomas") with a wide morphological spectrum. Am J Pathol, 1998. 153(3): p. 875-86.

29.   Okuwaki, M., The structure and functions of NPM1/Nucleophsmin/B23, a multifunctional nucleolar acidic protein. J Biochem, 2008. 143(4): p. 441-8.

30.   Fujimoto, J., et al., Characterization of the transforming activity of p80, a hyperphosphorylated protein in a Ki-1 lymphoma cell line with chromosomal translocation t(2;5). Proc Natl Acad Sci U S A, 1996. 93(9): p. 4181-6.

31.   Bischof, D., et al., Role of the nucleophosmin (NPM) portion of the non-Hodgkin's lymphoma-associated NPM-anaplastic lymphoma kinase fusion protein in oncogenesis. Mol Cell Biol, 1997. 17(4): p. 2312-25.

32.   Kuefer, M.U., et al., Retrovirus-mediated gene transfer of NPM-ALK causes lymphoid malignancy in mice. Blood, 1997. 90(8): p. 2901-10.

33. Bai, R.Y., et al., Nucleophosmin-anaplastic lymphoma kinase of large-cell anaplastic lymphoma is a constitutively active tyrosine kinase that utilizes phospholipase C-gamma to mediate its mitogenicity. Mol Cell Biol, 1998. 18(12): p. 6951-61.

34. Chiarle, R., et al., NPM-ALK transgenic mice spontaneously develop T-cell lymphomas and plasma cell tumors. Blood, 2003. 101(5): p. 1919-27.

35. Turner, S.D. and D.R. Alexander, What have we learnt from mouse models of NPM-ALK-induced lymphomagenesis? Leukemia, 2005. 19(7): p. 1128-34.

36. Tabbo, F., et al., ALK Signaling and Target Therapy in Anaplastic Large Cell Lymphoma. Front Oncol, 2012. 2: p. 41.

37. Zamo, A., et al., Anaplastic lymphoma kinase (ALK) activates Stat3 and protects hematopoietic cells from cell death. Oncogene, 2002. 21(7): p. 1038-47.

38. Chiarle, R., et al., Stat3 is required for ALK-mediated lymphomagenesis and provides a possible therapeutic target. Nat Med, 2005. 11(6): p. 623-9.

39. Amin, H.M., et al., Inhibition of JAK3 induces apoptosis and decreases anaplastic lymphoma kinase activity in anaplastic large cell lymphoma. Oncogene, 2003. 22(35): p. 5399-407.

40. Nieborowska-Skorska, M., et al., Role of signal transducer and activator of transcription 5 in nucleophosmin/ anaplastic lymphoma kinase-mediated malignant transformation of lymphoid cells. Cancer Res, 2001. 61(17): p. 6517-23.

41. Zhang, Q., et al., STAT5A is epigenetically silenced by the tyrosine kinase NPM1-ALK and acts as a tumor suppressor by reciprocally inhibiting NPM1-ALK expression. Nat Med, 2007. 13(11): p. 1341-8.

42. Hallberg, B. and R.H. Palmer, Mechanistic insight into ALK receptor tyrosine kinase in human cancer biology. Nat Rev Cancer, 2013. 13(10): p. 685-700.

43. Sakamoto, K., et al., ALK-positive large B-cell lymphoma: identification of EML4-ALK and a review of the literature focusing on the ALK immunohistochemical staining pattern. Int J Hematol, 2016. 103(4): p. 399-408.

44. Hubinger, G., et al., Hammerhead ribozyme-mediated cleavage of the fusion transcript NPM-ALK associated with anaplastic large-cell lymphoma. Exp Hematol, 2003. 31(3): p. 226-33.

45. Piva, R., et al., Ablation of oncogenic ALK is a viable therapeutic approach for anaplastic large-cell lymphomas. Blood, 2006. 107(2): p. 689-97.

46. Wan, W., et al., Anaplastic lymphoma kinase activity is essential for the proliferation and survival of anaplastic large-cell lymphoma cells. Blood, 2006. 107(4): p. 1617-23.

47. Galkin, A.V., et al., Identification of NVP-TAE684, a potent, selective, and efficacious inhibitor of NPM-ALK. Proc Natl Acad Sci U S A, 2007. 104(1): p. 270-5.

48. Li, R. and S.W. Morris, Development of anaplastic lymphoma kinase (ALK) small-molecule inhibitors for cancer therapy. Med Res Rev, 2008. 28(3): p. 372-412.

49. Cheng, M. and G.R. Ott, Anaplastic lymphoma kinase as a therapeutic target in anaplastic large cell lymphoma, non-small cell lung cancer and neuroblastoma. Anticancer Agents Med Chem, 2010. 10(3): p. 236-49.

50. Kwak, E.L., et al., Anaplastic lymphoma kinase inhibition in non-small-cell lung cancer. N Engl J Med, 2010. 363(18): p. 1693-703.

51. Gambacorti-Passerini, C., C. Messa, and E.M. Pogliani, Crizotinib in anaplastic large-cell lymphoma. N Engl J Med, 2011. 364(8): p. 775-6.

52. Cui, J.J., et al., Structure based drug design of crizotinib (PF-02341066), a potent and selective dual inhibitor of mesenchymal-epithelial transition factor (c-MET) kinase and anaplastic lymphoma kinase (ALK). J Med Chem, 2011. 54(18): p. 6342-63.

53. Zou, H.Y., et al., An orally available small-molecule inhibitor of c-Met, PF-2341066, exhibits cytoreductive antitumor efficacy through antiproliferative and antiangiogenic mechanisms. Cancer Res, 2007. 67(9): p. 4408-17.

54. Christensen, J.G., et al., Cytoreductive antitumor activity of PF-2341066, a novel inhibitor of anaplastic lymphoma kinase and c-Met, in experimental models of anaplastic large-cell lymphoma. Mol Cancer Ther, 2007. 6(12 Pt 1): p. 3314-22.

55. Mologni, L., Inhibitors of the anaplastic lymphoma kinase. Expert Opin Investig Drugs, 2012. 21(7): p. 985-94.

56. Leeman, R.J., V.W. Lui, and J.R. Grandis, STAT3 as a therapeutic target in head and neck cancer. Expert Opin Biol Ther, 2006. 6(3): p. 231-41.

57. Frank, D.A., STAT3 as a central mediator of neoplastic cellular transformation. Cancer Lett, 2007. 251(2): p. 199-210.

58. Darnell, J.E., Jr., I.M. Kerr, and G.R. Stark, Jak-STAT pathways and transcriptional activation in response to IFNs and other extracellular signaling proteins. Science, 1994. 264(5164): p. 1415-21.

59. Darnell, J.E., Jr., The JAK-STAT pathway: summary of initial studies and recent advances. Recent Prog Horm Res, 1996. 51: p. 391-403; discussion 403-4.

60. Fagard, R., et al., STAT3 inhibitors for cancer therapy: Have all roads been explored? JAKSTAT, 2013. 2(1): p. e22882.

61. Xiong, A.L., et al., Transcription Factor STAT3 as a Novel Molecular Target for Cancer Prevention. Cancers, 2014. 6(2): p. 926-957.

62. Vogt, M., et al., The role of the N-terminal domain in dimerization and nucleocytoplasmic shuttling of latent STAT3. J Cell Sci, 2011. 124(Pt 6): p. 900-9.

63. Braunstein, J., et al., STATs dimerize in the absence of phosphorylation. J Biol Chem, 2003. 278(36): p. 34133-40.

64. Santoni, M., et al., Investigational therapies targeting signal transducer and activator of transcription 3 for the treatment of cancer. Expert Opin Investig Drugs, 2015. 24(6): p. 809-24.

65. Becker, S., B. Groner, and C.W. Muller, Three-dimensional structure of the Stat3beta homodimer bound to DNA. Nature, 1998. 394(6689): p. 145-51.

66. Sgrignani, J., et al., Structural Biology of STAT3 and Its Implications for Anticancer Therapies Development. Int J Mol Sci, 2018. 19(6).

67. Arora, L., et al., The Role of Signal Transducer and Activator of Transcription 3 (STAT3) and Its Targeted Inhibition in Hematological Malignancies. Cancers (Basel), 2018. 10(9).

68. Beebe, J.D., J.Y. Liu, and J.T. Zhang, Two decades of research in discovery of anticancer drugs targeting STAT3, how close are we? Pharmacol Ther, 2018. 191: p. 74-91.

69. Yuan, J., F. Zhang, and R. Niu, Multiple regulation pathways and pivotal biological functions of STAT3 in cancer. Sci Rep, 2015. 5: p. 17663.

70. Catlett-Falcone, R., W.S. Dalton, and R. Jove, STAT proteins as novel targets for cancer therapy. Signal transducer an activator of transcription. Curr Opin Oncol, 1999. 11(6): p. 490-6.

71. Bowman, T., et al., STATs in oncogenesis. Oncogene, 2000. 19(21): p. 2474-88.

72. Yu, H., et al., Revisiting STAT3 signalling in cancer: new and unexpected biological functions. Nat Rev Cancer, 2014. 14(11): p. 736-46.

73. Xu, D. and C.K. Qu, Protein tyrosine phosphatases in the JAK/STAT pathway. Front Biosci, 2008. 13: p. 4925-32.

74. Linossi, E.M. and S.E. Nicholson, Kinase inhibition, competitive binding and proteasomal degradation: resolving the molecular function of the suppressor of cytokine signaling (SOCS) proteins. Immunol Rev, 2015. 266(1): p. 123-33.

75. Krebs, D.L. and D.J. Hilton, SOCS proteins: negative regulators of cytokine signaling. Stem Cells, 2001. 19(5): p. 378-87.

76. Chung, C.D., et al., Specific inhibition of Stat3 signal transduction by PIAS3. Science, 1997. 278(5344): p. 1803-5.

77. Silva, C.M., Role of STATs as downstream signal transducers in Src family kinase-mediated tumorigenesis. Oncogene, 2004. 23(48): p. 8017-8023.

78. Koskela, H.L., et al., Somatic STAT3 mutations in large granular lymphocytic leukemia. N Engl J Med, 2012. 366(20): p. 1905-13.

79. Couronne, L., et al., STAT3 mutations identified in human hematologic neoplasms induce myeloid malignancies in a mouse bone marrow transplantation model. Haematologica, 2013. 98(11): p. 1748-52.

80. Crescenzo, R., et al., Convergent mutations and kinase fusions lead to oncogenic STAT3 activation in anaplastic large cell lymphoma. Cancer Cell, 2015. 27(4): p. 516-32.

81. Vainchenker, W., et al., JAK inhibitors for the treatment of myeloproliferative neoplasms and other disorders. F1000Res, 2018. 7: p. 82.

82. Turkson, J., et al., Phosphotyrosyl peptides block Stat3-mediated DNA binding activity, gene regulation, and cell transformation. J Biol Chem, 2001. 276(48): p. 45443-55.

83. Coleman, D.R.t., et al., Investigation of the binding determinants of phosphopeptides targeted to the SRC homology 2 domain of the signal

transducer and activator of transcription 3. Development of a high-affinity peptide inhibitor. J Med Chem, 2005. 48(21): p. 6661-70.

84. Gunning, P.T., et al., Isoform selective inhibition of STAT1 or STAT3 homo-dimerization via peptidomimetic probes: structural recognition of STAT SH2 domains. Bioorg Med Chem Lett, 2007. 17(7): p. 1875-8.

85. Johnson, D.E., R.A. O'Keefe, and J.R. Grandis, Targeting the IL-6/JAK/STAT3 signalling axis in cancer. Nat Rev Clin Oncol, 2018. 15(4): p. 234-248.

86. Yang, J. and G.R. Stark, Roles of unphosphorylated STATs in signaling. Cell Res, 2008. 18(4): p. 443-51.

87. Sakamoto, K.M., et al., Protacs: chimeric molecules that target proteins to the Skp1-Cullin-F box complex for ubiquitination and degradation. Proc Natl Acad Sci U S A, 2001. 98(15): p. 8554-9.

88. Hochstrasser, M., Ubiquitin, proteasomes, and the regulation of intracellular protein degradation. Curr Opin Cell Biol, 1995. 7(2): p. 215-23.

89. Navon, A. and A. Ciechanover, The 26 S proteasome: from basic mechanisms to drug targeting. J Biol Chem, 2009. 284(49): p. 33713-8.

90. Pettersson, M. and C.M. Crews, PROteolysis TArgeting Chimeras (PROTACs) - Past, present and future. Drug Discov Today Technol, 2019. 31: p. 15-27.

91. Bai, L., et al., A Potent and Selective Small-Molecule Degrader of STAT3 Achieves Complete Tumor Regression In Vivo. Cancer Cell, 2019. 36(5): p. 498-511 e17.

92. Heppler, L.N. and D.A. Frank, Inhibit versus Destroy: Are PROTAC Degraders the Solution to Targeting STAT3? Cancer Cell, 2019. 36(5): p. 459-461.

93. Cobb, L.M., The behaviour of carcinoma of the large bowel in man following transplantation into immune deprived mice. Br J Cancer, 1973. 28(5): p. 400-11.

94. Crystal, A.S., et al., Patient-derived models of acquired resistance can identify effective drug combinations for cancer. Science, 2014. 346(6216): p. 1480-1486.

95.   Fiore, D., et al., Patient-Derived-Tumor-Xenograft: modeling cancer for basic and translational cancer research. Clinical and Diagnostic Pathology, 2017. 1(2).

96.   Ito, M., et al., NOD/SCID/gamma(c)(null) mouse: an excellent recipient mouse model for engraftment of human cells. Blood, 2002. 100(9): p. 3175-82.

97.   Racki, W.J., et al., NOD-scid IL2rgamma(null) mouse model of human skin transplantation and allograft rejection. Transplantation, 2010. 89(5): p. 527-36.

98.   Pineda, G., et al., Tracking of Normal and Malignant Progenitor Cell Cycle Transit in a Defined Niche. Sci. Rep. 6, 23885; (2016).

99.   Mak, V., et al., Su.rvival of patients with peripheral T-cell lymphoma after first relapse or progression: spectrum of disease and rare long-term survivors. J. Clin. Oncol. 31, 1970–1976 (2013).

100.   Iqbal, J., et al., Genomic signatures in T-cell lymphoma: How can these improve precision in diagnosis and inform prognosis? Blood Rev. 2016;30:89–100.